Università
di Genova

Development of new, potent NAPRT inhibitors by CADD

Dissertation for the Acquisition of a Doctoral Degree
at the Department of Haemato-Oncology and Clinical-Translational Internal Medicine of
The University of Genoa

Submitted by

Jorge Franco

December 2022

1st reviewer: Prof. Dr. Alessio Nencioni

2nd reviewer: Prof. Dr. Santina Bruzzone

3rd reviewer: Dr. Alberto Del Rio

Table of Contents

ABSTRACT

Nicotinate phosphoribosyltransferase (NAPRT) is the rate-limiting enzyme of the Preiss-Handler NAD biosynthetic pathway. NAPRT is widely distributed across healthy mammalian tissues where the enzyme supports the production of NAD, an essential pyridine nucleotide that acts as redox cofactor in multiple metabolic pathways key for bioenergetics and as substrate for several critical cellular processes.

Recently, NAPRT has emerged as a novel therapeutic target against cancer owing to its recognition as a biomarker for the success of NAMPT inhibitors in cancer treatment. Indeed, the lack of objective tumor response to NAMPT inhibitors in clinical trials might reflect NAPRT-mediated resistance to these agents. Interestingly, NAPRT displays marked tumor specificity in terms of expression and its regulation mechanisms. Some tumors show NAPRT gene promoter hypermethylation and therefore do not express the enzyme. An insightful study found that NAPRT is frequently upregulated in ovarian, prostate, pancreatic, and breast cancers. In addition, high protein levels of NAPRT were shown to confer resistance to NAMPT inhibitors in several tumor types whereas the simultaneous inhibition of NAMPT and NAPRT resulted in marked anti-tumor effects both *in vitro* and *in vivo*.

While numerous potent NAMPT inhibitors are available, the few reported NAPRT inhibitors (NAPRTi) have a low affinity for the enzyme. In this work, computer-aided drug design (CADD) efforts to identify putative NAPRT inhibitors were coupled to state-of-the-art *in vitro* testing of the compounds to study their capacity to inhibit NAPRT and to sensitize the NAPRT-proficient OVCAR-5 cell line to the NAMPTi FK866. Starting from the crystal structure of NAPRT several structure-based drug design (SBDD) experiments based on molecular docking and molecular dynamics simulations were carried out. In the process, large compound libraries of diverse and drug-like small molecules were virtually screened against the NAPRT structure. The selected *in silico* hits were subsequently tested through cell-based assays in the NAPRT-proficient OVCAR-5 ovarian carcinoma cell line and on the recombinant NAPRT enzyme. We found different chemotypes that efficiently inhibit the enzyme in the micromolar range concentration and for which direct engagement with the target was verified by differential scanning fluorimetry. Of note, the therapeutic potential of these compounds was evidenced by a synergistic interaction between the NAMPT inhibitor FK866 and the new NAPRTi in terms of decreasing OVCAR-5 intracellular NAD^+ levels and cell viability. For example, compound IM 29 can potentiate the effect of FK866 of more than two-fold in reducing intracellular NAD^+

levels. These results pave the way for the development of a new generation of potent NAPRT inhibitors with anticancer activity.

LIST OF ABBREVIATIONS

Å	Angstrom
%	Percentage
°C	Celsius degree
μg	Microgram
μL	Microlitre
μM	Micromolar
Aa	Amino acid
ATP	Adenosine triphosphate
cADPR	Cyclic ADP-ribose
CADD	Computer-aided drug design
CI	Combination index
3D	Three-dimensional
DMSO	Dimethyl sulfoxide
DNA	Deoxyribonucleic acid
DSF	Differential scanning fluorimetry
EMT	Epithelial-mesenchymal transition
e.g.	Example
FBS	Fetal bovine serum
g	Gram
H_2O	Water
HTS	High-throughput screening
2-HNA	2-hydroxynicotinic acid
i.e.	*Id est*
IC_{50}	Half maximal inhibitory concentration
IDH1	Isocitrate dehydrogenase 1 genes
LBDD	Ligand-based drug design
logP	Partition coefficient
Mg^{2+}	Magnesium ion
mRNA	Messenger ribonucleic acid
NAPRTi	NAPRT inhibitors
Nam	Nicotinamide

NAD	Nicotinamide adenine dinucleotide
NAD^+	Oxidized nicotinamide adenine dinucleotide
$NADP^+$	Phosphorylated nicotinamide adenine dinucleotide
NA	Nicotinic acid
NAMN	Nicotinic acid mononucleotide
NAMPT	Nicotinamide phosphoribosyltransferase
NMNAT	Nicotinamide mononucleotide adenylyltransferase
NAPRT	Nicotinate phosphoribosyltransferase
hNAPRT	Human nicotinate phosphoribosyltransferase
NAR	Nicotinic acid riboside
NR	Nicotinamide riboside
NADSYN	Nicotinamide adenine dinucleotide synthetase
nM	Nanomolar
ns	Nanosecond
N/O atoms	Nitrogen or Oxygen atoms
pH	Power of hydrogen
PARPs	Poly-(ADP–ribose) polymerases
PCA	Perchloric acid
PDB	Protein data bank
PPi	Pyrophosphate
PPM1D	Protein phosphatase Mg^{2+}/Mn^{2+}-dependent 1D
PRPP	5-phosphoribosyl-1-pyrophosphate
Ps	Picosecond
PSA	Polar surface area
QA	Quinolinic acid
QPRT	Quinolinate phosphoribosyltransferase
QSAR	Quantitative structure-activity relationship
RMSD	Root mean square deviation
RPMI	Roswell Park Memorial Institute
SARM1	Sterile alpha and TIR motif-containing 1
SBDD	Structure-based drug design
SEM	Standard error of the means
SIRT1-7	Sirtuins

SRB	Sulforhodamine B
TCA cycle	Tricarboxylic acid cycle
Tm	Melting temperature
Trp	Tryptophan
vHTS	Virtual high-throughput screening
VS	Virtual screening
X-ray	X-radiation

1. INTRODUCTION

1.1 Physiological roles of NAD

Nicotinamide adenine dinucleotide (NAD) is a vital pyridine nucleotide. The first role that was discovered for NAD^+ and its phosphorylated form ($NADP^+$) was as an essential coenzyme in redox reactions that are involved in cell energy and anabolic metabolism. By exchanging hydride, $NAD(P)^+$ is constantly shuttling between its oxidized and reduced forms in hundreds of enzymatic reactions that take part in key pathways in mammalian cells, such as glycolysis, tricarboxylic acid cycle (TCA cycle), oxidative phosphorylation, and serine biosynthesis [1–3]. Besides, the reduced form of phosphorylated NAD (NADPH) is particularly relevant for the cell's defense against oxidative stress as it provides the reductive power to neutralize reactive oxygen species [4]. In addition, marked cell regulatory properties have been ascribed to NAD by acting as a substrate for several families of enzymes, which always release nicotinamide (Nam) as a result of NAD degradation [1,5–7]. Indeed, NAD is consumed in post-translational modifications of target proteins by mono- and poly-(ADP–ribose) polymerases (PARPs) and sirtuins (SIRT1-7), the last endowed with protein deac(et)ylase activity [8,9]. NAD is also the precursor of the Ca^{2+}-mobilizing second messenger cyclic ADP-ribose (cADPR), produced by the ectoenzymes CD38 and CD157 [10]. The enzyme sterile alpha and TIR motif-containing 1 (SARM1) exerts NAD-cleavage activity in neurons and represents a new family of NAD-consuming enzymes [11]. The activities of these enzymes are modulated by NAD availability and regulate a series of fundamental cellular processes including DNA repair, apoptosis, cell metabolism, cell cycle progression, and immune responses [12].

1.2 NAD biosynthesis in human

Unlike a redox cofactor, NAD is consumed when acting as a substrate. Therefore, continuous NAD biosynthesis is required in normal human tissues to preserve NAD homeostasis and thus health [13]. As a matter of fact, the decline in NAD levels during ageing is related with the development of an array of metabolic disorders and diseases, including cancer [6]. Due to aberrant metabolism, cell growth, and proliferation, tumor cells require higher NAD production with respect to healthy tissues to support the increased activity of NAD-degrading enzymes [14]. Therefore, interfering with the NAD biosynthetic machinery was conceived as a promising therapeutic strategy against cancer [12,15]. The depletion of NAD strongly affects multiple cellular metabolic pathways, leads to a rapid decline in adenosine triphosphate (ATP)

levels, and ultimately causes cancer cell death [16]. For a more detailed overview of the *in vitro* and *in vivo* effects of chemical agents targeting NAD biosynthesis in cancer cells, we refer the readers to a recent review article [17].

There are three main pathways contributing to NAD biosynthesis in mammals, which show high tissue variability: the de novo pathway with tryptophan as a NAD precursor, the Preiss–Handler pathway, which utilizes nicotinic acid (NA) as a starting block, and the nicotinamide (Nam) salvage pathway (Figure 1) [18]. In addition, the ribosylated precursors nicotinamide riboside (NR) and nicotinic acid riboside (NAR) represent additional forms of vitamin B3 that can be converted into NAD. All known routes leading to NAD generation in human require the transfer of the adenylyl moiety contained in ATP to nicotinamide mononucleotide (NMN) or nicotinic acid mononucleotide (NAMN), evidencing the essentiality of the NMNAT activity. In humans, 3 NMNAT isoforms (NMNAT1-3) fine-tune NAD synthesis in tissues and intracellular organelles [19].

The Nam salvage pathway plays a key role in maintaining NAD homeostasis in mammalian cells [20]. Duarte-Pereira and colleagues observed that the gene of the rate-limiting enzyme of this pathway, nicotinamide phosphoribosyltransferase (NAMPT), was ubiquitously expressed at the mRNA level in all human normal tissues and tumors that were studied [21]. Moreover, NAD-consuming enzymes release nicotinamide as a by-product, which makes Nam the most accessible NAD precursor. The protagonism that the Nam salvage pathway holds within the animal kingdom does not apply to distant forms of life. A detailed analysis of the genoma of 45 species covering very different organisms from the tree of life concluded that the three enzymes of the Preiss-Handler pathway (i.e., NAPRT, NMNAT and NADS) are detected in all the species investigated except *H. influenzae* and *M. jannaschii* [22]. In contrast, NAMPT is frequently absent outside animals and replaced by nicotinamidase activity coupled to the PH pathway.

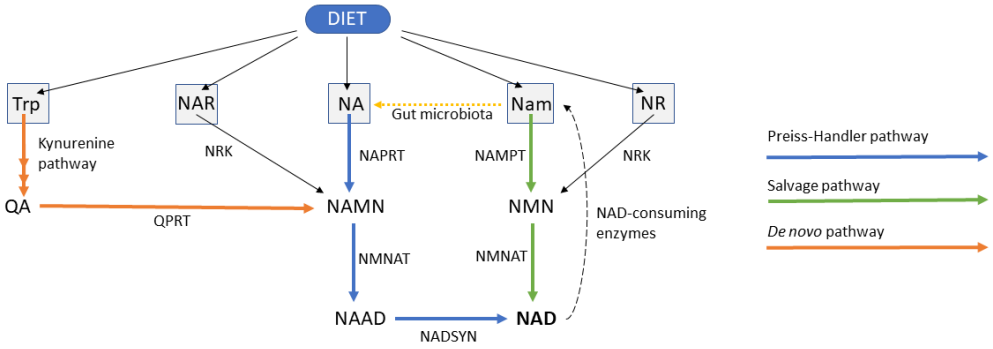

Figure 1 Graphical depiction of NAD biosynthesis in mammals. Trp, tryptophan; NA, nicotinic acid; NAR, nicotinic acid riboside; NR, nicotinamide riboside; Nam, nicotinamide; QA, quinolinic acid; NAMN, nicotinic acid mononucleotide; NMN, nicotinamide mononucleotide; NAAD, nicotinic acid adenine dinucleotide; NAD, nicotinamide adenine dinucleotide; QPRT, quinolinate phosphoribosyltransferase; NAPRT, nicotinate phosphoribosyltransferase; NAMPT, nicotinamide phosphoribosyltransferase; NRK, nicotinamide riboside kinase; NMNAT, nicotinamide mononucleotide adenylyltransferase; NADSYN, nicotinamide adenine dinucleotide synthetase.

1.2.1 Nicotinate phosphoribosyltransferase

Human nicotinate phosphoribosyltransferase (hNAPRT, Uniprot: Q6XQN6) is the rate-limiting enzyme of the Preiss–Handler pathway. The enzyme catalyzes the conversion of NA and 5-phosphoribosyl-1-pyrophosphate (PRPP) to NAMN and pyrophosphate (PPi) in an ATP-dependent manner [23]. The Preiss–Handler pathway continues with the adenylation of NAMN catalyzed by NMNAT1-3 and ends with the amidation of nicotinic acid adenine dinucleotide (NAAD) to NAD, which is catalyzed by NAD synthetase (NADSYN). Human NAPRT belongs to the Type II phosphoribosyltransferase family of functional dimeric proteins that are involved in NAD biosynthesis, together with quinolinate phosphoribosyltransferase (QPRT) and NAMPT. The crystal structure of NAPRT was solved by Marletta *et al*. and evidenced that the NAPRT monomer consists of an irregular α/β barrel domain and of a second open-faced sandwich domain [24].

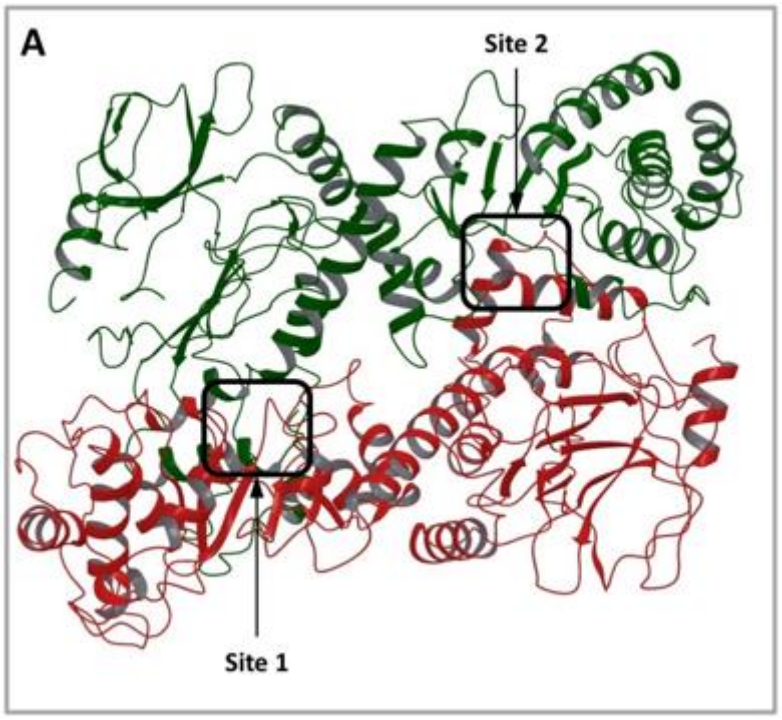

Figure 2. Dimeric structure of hNAPRT. Monomer A is depicted in green and monomer B in red. The two active sites located at the dimer interface are highlighted.

Despite the low sequence similarity between hNAPRT and its bacterial homologs, the main amino acids that are involved in the recognition of NAPRT substrates and catalysis are strictly conserved, as demonstrated through site-directed mutagenesis experiments (Table 1) [25].

Table 1. Mutagenesis studies performed on hNAPRT enzymatic activity.

Mutation position	Effect on activity
19; Asp-Ala	Total loss
21; Try-Ala	Partial loss w/ATP, total loss w/o ATP
169; Gly-Ala	Partial loss
209; Gly-Ala	Partial loss
213; His-Ala	Partial loss
288; Asp-Ala	Total loss
318; Arg-Ala	Partial loss w/ATP, total loss w/o ATP
357; Asn-Ala	Small loss
379; Gly-Ala	Total loss
380; Thr-Ala	Partial loss
381; Ser-Ala	Partial loss

NAPRT displays marked tissue and tumor specificity in terms of expression and its regulation mechanisms and is mostly present in several catabolic healthy mammalian tissues including the heart, kidney, liver, and small intestine [21,26–30]. In tissues that express the NAPRT protein, NA is the preferred precursor of NAD. Accordingly, the NAD pool of HEK293 cells

was dramatically increased when these were cultured in NA-rich conditions, whereas similar doses of Nam resulted in a much lower effect [30]. This observation is likely related to the fact that, unlike NAMPT, NAPRT activity is not inhibited by NAD [30]. Interestingly, in addition to the role of NAMPT and NAPRT as intracellular NAD-producing enzymes (mostly located in the nucleus and the cytoplasm), NAMPT and NAPRT also exist as extracellular proteins, which exert pro-inflammatory and pro-tumorigenic effects [15,31,32].

1.3 NAD depletion as an anticancer strategy

1.3.1 Inhibition of NAMPT

Since interfering with NAD biosynthesis emerged as a viable strategy in oncology, the search for inhibitors has largely focused on NAMPT and led to the identification of numerous inhibitors, including FK866, CHS-828, OT-82, and KPT-9274 [33–37]. NAMPT is highly expressed in a broad range of both solid and hematological cancers, such as pancreatic cancer, ovarian cancer, colorectal cancer and lymphomas. Given the nature of NAMPT as the rate-limiting enzyme of the Nam salvage pathway, an increased activity of this enzyme typically translates into poor cancer prognosis [38].

Interestingly, potent NAMPTi have demonstrated very efficient anticancer activity *in vitro* and *in vivo*. The particular mechanism by which cancer cells die in response to NAMPT inhibitors seems to depend on the NAMPTi used and the cancer type and can consist of apoptosis, autophagy or oncosis. NAMPT inhibitors exert their cytotoxic effects through NAD depletion that ultimately impacts multiple cellular processes. The main downstream effects of NAD depletion are impairment of glycolysis and ATP depletion, mitochondrial depolarization, plasma membrane disintegration and genome vulnerability. The genome vulnerability is due to decreased PARP activity and a reduced antioxidant capacity of the cell as a result of NADPH depletion with the corresponding increase in reactive oxygen species that cause DNA damage. Accordingly, NAMPTi effectively cooperate with DNA damage-inducing chemicals like fludarabine and cisplatin. Inhibition of NAMPT also synergizes with other anticancer therapies such as radiotherapy and immunotherapy.

Multiple studies report the *in vivo* efficacy of several NAMPTi. In theory, coadministration of NA with NAMPT inhibitors to patients with NAPRT-deficient tumors should mitigate the systemic toxicity associated with NAMPTi without rescuing the tumor cells [39,40]. Indeed, this is the case in several *in vivo* studies. In contrast, tumors in which the Preiss-Handler NAD

synthetic pathway is amplified would require simultaneous inhibition of NAMPT and NAPRT to reach dramatic NAD depletion and cell death in the cancers. Strikingly, a loss of NAMPTi antitumor activity in NAPRT-negative malignancies has also been reported upon NA supplementation [41]. This outcome shows that the efficacy of NAD depletion treatments *in vivo* is difficult to predict as a result of the complexity of the human body, where organs cooperate to synthesize NAD and the NAD metabolites are in continuous exchange.

Overall, the first generation NAMPT inhibitors achieved potent antitumor activity in preclinical models. Nevertheless, the efficacy of these compounds in clinical trials has been rather disappointing. The NAMPT inhibitors failed to evoke an objective tumor response and, in addition, thrombocytopenia and gastrointestinal symptoms arose as dose-limiting toxicities [42,43]. Studies show that the upregulation of the Preiss-Handler pathway in tumors could be responsible for the limited clinical activity of the NAMPTi tested [26,44].

1.3.2 NAPRT as a therapeutic target

The enzyme NAPRT emerged as a promising therapeutic target for cancer treatment when it was proposed and demonstrated that inhibition of NAPRT is necessary to sensitize NAPRT-proficient malignancies to the NAMPT inhibitor FK866 both *in vitro* and *in vivo* [26]. The same authors elucidated the results of NAPRT silencing or inhibition in the tumor types tested: reduced cytosolic and mitochondrial NAD levels, decreased intracellular ATP, decreased oxidative phosphorylation, and reduced protein synthesis.

With respect to the amplification of the NAPRT gene and to its expression, these are very variable in human tumors [21,26,28]. Tumors originating from normal tissues that highly express NAPRT were found to amplify the NAPRT gene at a high frequency (and to express it at high levels as a result), whereas tumors arising from tissues that do not express NAPRT will strongly rely on NAMPT activity for NAD biosynthesis and for cell survival [28]. In ovarian, prostate, breast, and pancreatic cancers, NAPRT was found upregulated (Figure 3A) [26]. On the contrary, gastric, renal, and colorectal carcinoma, as well as several leukemia cell lines, were reported to have low or no NAPRT expression [21].

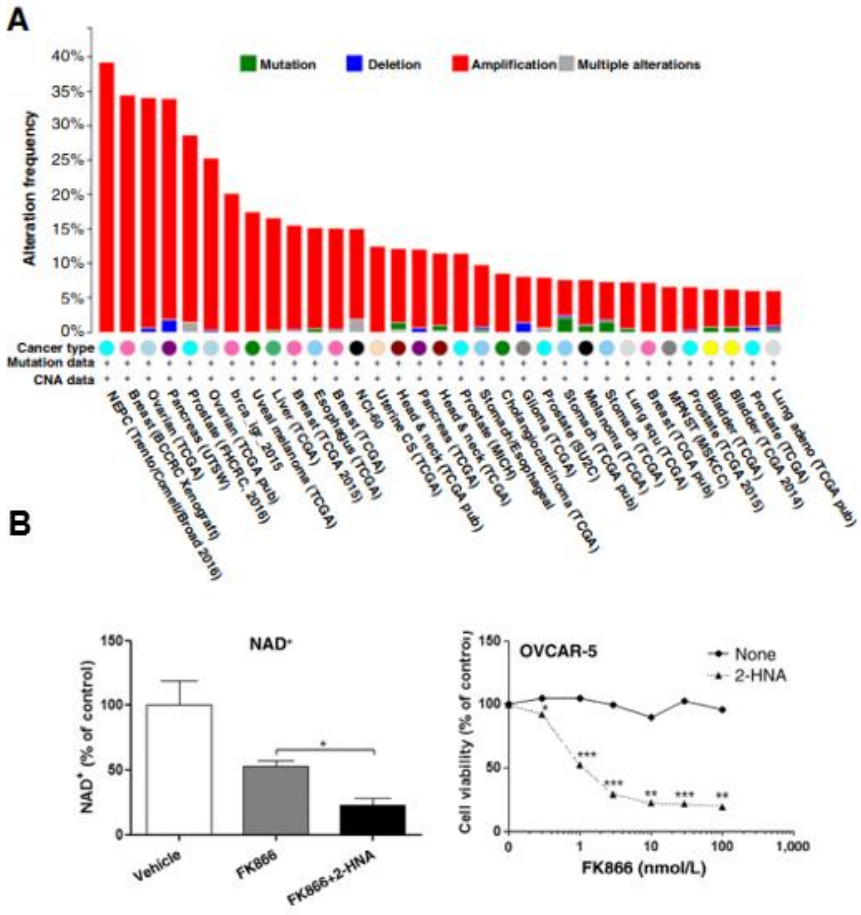

Figure 3. A, NAPRT is frequently amplified in a subset of human tumors. B, Synergistic interaction between FK866 and 2-HNA in impairing cell viability and decreasing NAD⁺ of OVCAR-5 cells. This figure is adopted from Piacente et al., 2017[26]

Among the mechanisms that regulate NAPRT expression, hypermethylation of the NAPRT gene promoter leads to gene silencing and has been found in several NAPRT-negative tumors. NAPRT promoter hypermethylation in cancer is frequently associated with mutations in the protein phosphatase Mg^{2+}/Mn^{2+}-dependent 1D (PPM1D) or isocitrate dehydrogenase 1 (IDH1) genes, as well as with the epithelial-mesenchymal transition (EMT)-subtype of gastric cancer [45–47]. Due to their dependency on the Nam salvage pathway for survival, NAPRT-deficient cancers are extremely sensitive to treatment with NAMPT inhibitors [48,49]. On the other hand, NAPRT upregulation confers resistance to NAMPT inhibitors to many malignancies. Piacente et al. demonstrated that NAPRT-proficient ovarian and pancreatic cancers are resistant to FK866, whereas NAPRT downregulation through gene silencing or chemical inhibition with 2-hydroxynicotinic acid (2-HNA) sensitized tumor cells to NAMPT inhibitors both *in vitro* and *in vivo* (Figure 3B) [26]. In line with these results, another study highlighted

that sensitivity to NAMPT inhibition in several ovarian cancer cell lines was inversely proportional to NAPRT expression [50]. Despite its usefulness in basic research as NAPRTi, the low molecular weight and high functionality of 2-hydroxynicotinic acid suggest that this compound could have non-specific effects. Together with its low potency, such features make it unlikely that 2-HNA could be utilized as a NAPRTi in the clinic.

1.3.3 Reported NAPRT inhibitors

Recently, two new molecules (compound 8 and compound 19) that were able to reproduce the anticancer activity of 2-HNA *in vitro* as NAPRT inhibitors, were reported (Ghanem *et al*., 2022). Additional NAPRT inhibitors date back to the 1970s, including nicotinic acid analogs and non-steroidal anti-inflammatory agents such as flufenamic acid, salicylic acid, mefenamic acid, and phenylbutazone (Table 2) [51–53]. Unfortunately, the available data, which were mostly obtained by monitoring NAPRT activity in human platelet lysates, suggest a weak inhibitory activity for these agents. Despite the proved antitumor activities of 2-HNA and compounds 8 and 19, efforts should be made in discovering new, potent NAPRT inhibitors. In this work, we identified several new small-molecule NAPRTi which, upon further compound optimization, could lead to a new generation of molecules that sensitize NAPRT-proficient malignancies to NAMPT inhibitors and, possibly, to other anticancer agents.

Table 2. hNAPRT inhibitors reported in the literature.

Compound	Apparent K_i (μM)
Flufenamic acid	10
Mefenamic acid	50
2-Phenylbutazone	75
Indomethacin	100
Salicylic acid	150
2-Hydroxynicotinic acid	160
2-Fluoronicotinic acid	230
Compound 19	295
Oxyphenbutazone	300
Compound 8	307.5
Acetylsalicylic acid	500
Sulfinpyrazone	500

1.4 Computer-aided drug design (CADD)

Computer-aided drug design (CADD) encompasses a broad and growing range of computational methodologies that assist in the various stages of drug development. CADD is chiefly used during the early phases of drug discovery, e.g., biological target assessment, hit identification and lead optimization. The staggering progress made in the last decades with regard to computational power alongside the continuous refinement of existing software have improved considerably the efficacy and costs of CADD efforts to the point that CADD is a key player in modern drug discovery. Indeed, CADD helps researchers minimize the synthetic and biological testing workload through high-speed computational methods that enrich the fraction of suitable lead candidates in a chemical database and is nowadays the most suitable alternative for high-throughput screening. The ensemble of CADD approaches allows to predict and modulate the properties (e.g., binding affinity, ADMET profile) of a compound in a defined biological system. Therefore, modern computational techniques have helped in achieving molecular-level understanding of biological processes, explaining the molecular basis of therapeutic activity. Another valuable contribution of CADD to the scientific community is the construction of high-quality datasets and libraries.

Roughly, CADD methodologies can be classified as structure-based drug design (SBDD) or ligand-based drug design (LBDD). SBDD exploits our knowledge of the target structure, e.g., experimentally solved X-ray crystal structure and homology modeling-derived structures. Examples of SBDD techniques are molecular docking and molecular dynamics (MD) simulations.

Contrary to SBDD, ligand-based drug design uses our knowledge of known active and inactive molecules. Among LBDD techniques there are similarity/substructure searches and quantitative structure-activity relationship (QSAR) models.

The choice of a certain CADD approach hinges upon the availability of structural features of the biological target and experimental data regarding the on-target activity of a set of ligands. In the case of a vastly studied enzyme, like NAMPT, both SBDD and LBDD are doable. On the contrary, a “young” enzyme whose therapeutic potential has only recently been discovered usually will be a greater challenge due to the limited data available. This is the case of hNAPRT.

1.4.1 Molecular docking

Molecular docking is a SBDD technique largely employed to identify and design compounds with strong binding affinity towards a target, by studying the binding free energy of the protein-ligand complex. Despite the ability of scoring functions to assign a numerical value to a binding pose, a thorough visual inspection of the binding pose is essential for a proper evaluation of the docking results. A critical aspect to consider when inspecting a binding pose and that reflect the actual binding ability of the ligand are the number, distribution, and directionality of intermolecular interactions (e.g., hydrogen bonds). It is also very important to evaluate the shape and electrostatic complementarity between the compound and the protein binding site. Another key parameter is the ligand strain in the predicted binding pose, which may suggest unrealistic ligand conformations.

Virtual high-throughput screening (vHTS) of large compound libraries via molecular docking is one of the most common applications of CADD. Among the computational tools that offer the possibility to perform docking-based virtual screening, AutoDock Vina is an open-source program that has been extensively tested and accurately predicts the binding mode of ligands within their target proteins. The workflow of a typical docking-based VS is depicted in Figure 4.

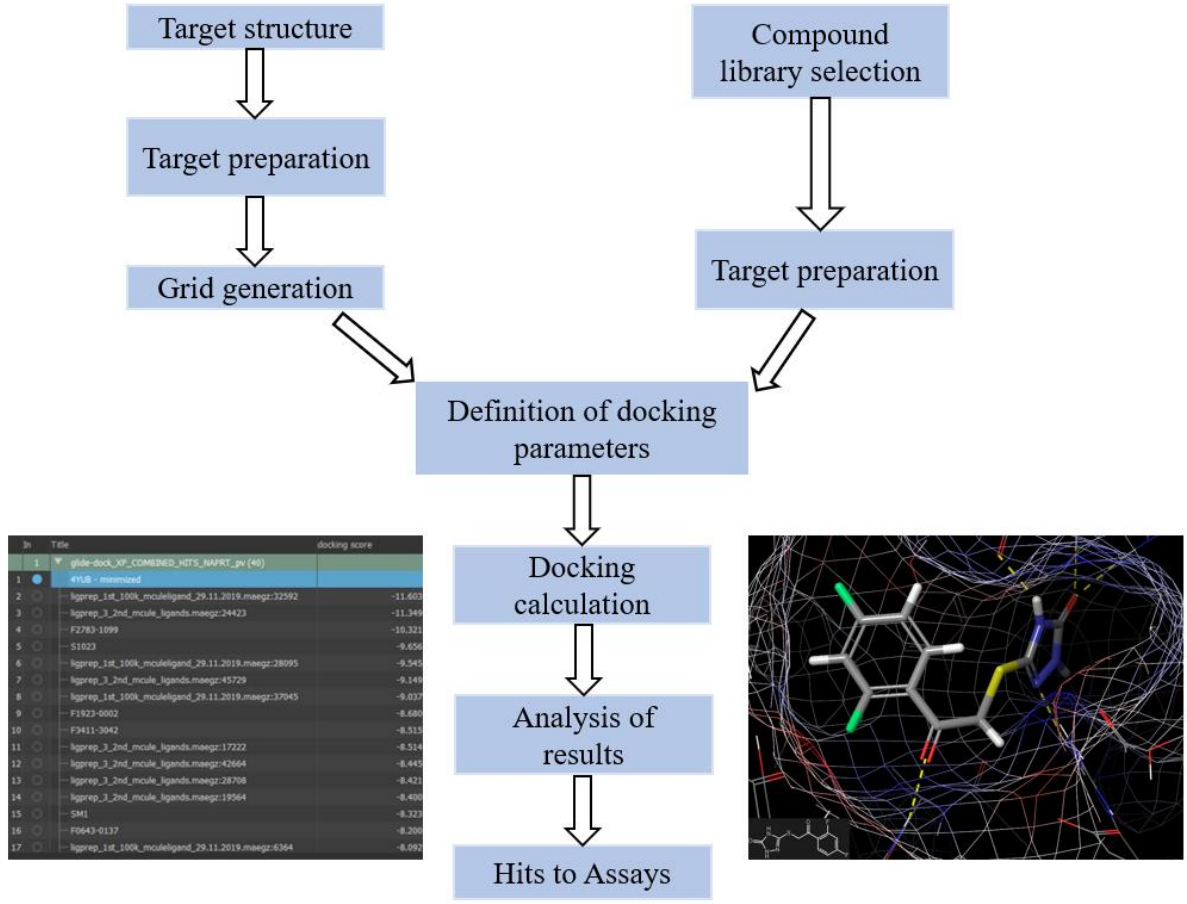

Figure 4. Typical vHTS workflow to follow when using molecular docking to identify inhibitors for a macromolecule.

Depending on the knowledge of existing small-molecule modulators of the target enzyme and the aim of the screening, the compound library subjected to docking will comprise more or less molecules with a higher or lower chemical diversity. Often, a large virtual compound library provided by a vendor or online platform is filtered according to Lipinski's rule of 5 or simple physicochemical properties to discard molecules with poor drug-likeness.

Afterwards, the ligands are prepared for docking, which means adding hydrogen atoms, generating their 3D structure, and sampling the protonation states at physiological pH and possible tautomers.

The target protein must as well undergo preparation in order to perform docking in a realistic system. Protein preparation comprises filling in missing amino acids and atoms, the removal of non-structural water molecules, the optimization of protonation states of ionizable residues, and a restrained energy minimization.

Next, the parameters for the docking experiment are defined. The docking grid is built around the receptor (target protein) binding site. Of note, the size and location of the grid box greatly impact the quality of the results. The user must as well specify the type of ligand sampling, the

scoring function, the precision level of docking, and the presence or absence of constraints. Once docking calculations have concluded, the user obtains a list of the top scoring binding poses from which docking hits will be selected via visual inspection.

1.4.2 Molecular dynamics simulations

Interestingly, enzymes are dynamic catalysts in an aqueous environment, meaning that the conformation of their binding sites evolves over time. The real movements of macromolecules in solution can be precisely reproduced by molecular dynamics (MD) simulations, a CADD technique that employs Newton's laws to produce the trajectories (i.e., atomic coordinates at specific time periods) of a system. An outstanding molecular dynamics package that executes high-performance simulations of proteins and output analysis is GROMACS.

One of the applications of MD simulations is to conduct conformational sampling, generating reasonable conformations of a macromolecule starting from its input structure (e.g., a PDB file of the crystal structure). These alternative enzyme conformations may well be used to run docking-based screening. The use of multiple docking grids enhances the chances of discovering inhibitors for an enzyme and is based on the dependence of intermolecular interactions with distance and directionality.

This thesis has relied on CADD to a large extent with the goal to identify new inhibitors of human nicotinate phosphoribosyltransferase (NAPRT). With this purpose, several SBDD approaches were attempted taking the X-ray-solved hNAPRT crystal structure as the starting point. Owing to the scarce information available on known NAPRT inhibitors, LBDD efforts may be more suitable in the future.

2. MATERIALS AND METHODS

2.1 Materials

Materials for the *in silico* experiments:
The modeling tools available in the Mcule online platform were used upon registration as a regular user. AutoDock Vina was used to perform the docking virtual screenings. The free, open-source program for ligand preparation (Gypsum-DL) and the free and open-source software for molecular dynamics (GROMACS) were used. Schrödinger's free Maestro v.2017-4 was used for *in silico* protein preparations and visual inspection of docking binding poses.

Materials for the *in vitro* experiments:
OVCAR-5 cells were obtained from the NCI-60 panel in 2015 as a kind gift from Prof. Zoppoli. The cells were passaged for less than six months before resuscitation for the experiments. Testing for mycoplasma was routinely done with the MycoAlert Mycoplasma Detection Kit (Lonza Group, Basel, Switzerland). The cells were maintained and treated with RPMI 1640 medium that was supplemented with 10% heat-inactivated FBS, penicillin (50 units/mL), and streptomycin (50 μg/mL) (Life Technologies, Monza, Italy). FK866 was kindly provided by the NIMH Chemical Synthesis and Drug Supply Program. 2-hydroxynicotinic acid was purchased (Sigma Aldrich S.r.l., Milan, Italy).

2.2 *In silico* identification of putative NAPRT inhibitors

2.2.1 Virtual screening on the crystal conformation of the NAPRT active site

A high-throughput molecular docking screening was performed to discover new inhibitors of hNAPRT. The crystal structure of NAPRT (PDB code: 4YUB) was retrieved from The Protein Data Bank [54]. This structure was prepared with the academic version of Schrodinger Maestro v.2017-4 with standard preparation procedures, that include the removal of water molecules, correct assignment of bond orders, the addition of hydrogens, and the optimization of protonation states and restrained energy minimization. A 15 Å grid centered on the enzymatically relevant active site residues LEU170A, ARG318A, and TYR21B was generated around the NAPRT active site [24,25].
The ligands subjected to docking were extracted from the Mcule "Potentially purchasable compounds" database. Approximately 1×10^5 molecules were selected after applying the physicochemical filter to the library (Table 3).

Table 3. Basic physicochemical parameters used in compound library filtering.

Property	Min. value	Max. value
Components	0	1
Inorganic atoms	0	0
Rotatable bonds	0	10
Chiral centers	0	3
Heavy atoms	8	
N/O atoms	1	15
Rings	1	
Halogen atoms	0	3
Mass	150	450
logP	0.4	5.6
PSA (Polar surface area)	70	140
Refractivity	160	480
H-bond donors	0	5
H-bond acceptors	1	8

Docking virtual screening was run with the modeling tools that are offered by the Mcule platform, performing ligand preparation with Gypsum-DL using the default settings [55,56]. The docking results were thoroughly visually inspected considering widely accepted aspects in the scientific community such as quality of ligand-receptor interactions, docking score, fitting in the active site, ligand strain, and drug-likeness [57]. About 20 compounds showed promising properties *in silico* and were purchased and tested *in vitro* as putative hNAPRT inhibitors.

2.2.2 Virtual screenings on NAPRT active site grids extracted from molecular dynamics simulations

A second high-throughput molecular docking screening was performed to discover new inhibitors of NAPRT. The crystal structure of NAPRT was subjected to a 100 ns molecular dynamics simulation in water on GROMACS, which is schematically described in Figure 5. The protein trajectory produced in the simulation was clustered and the most representative protein structure (at t = 70710 ps) was exported and prepared with the academic version of Schrodinger Maestro v.2017-4 with standard preparation procedures. A 15 Å grid centered on the enzymatically relevant active site residues LEU170A, ARG318A, and TYR21B was generated.

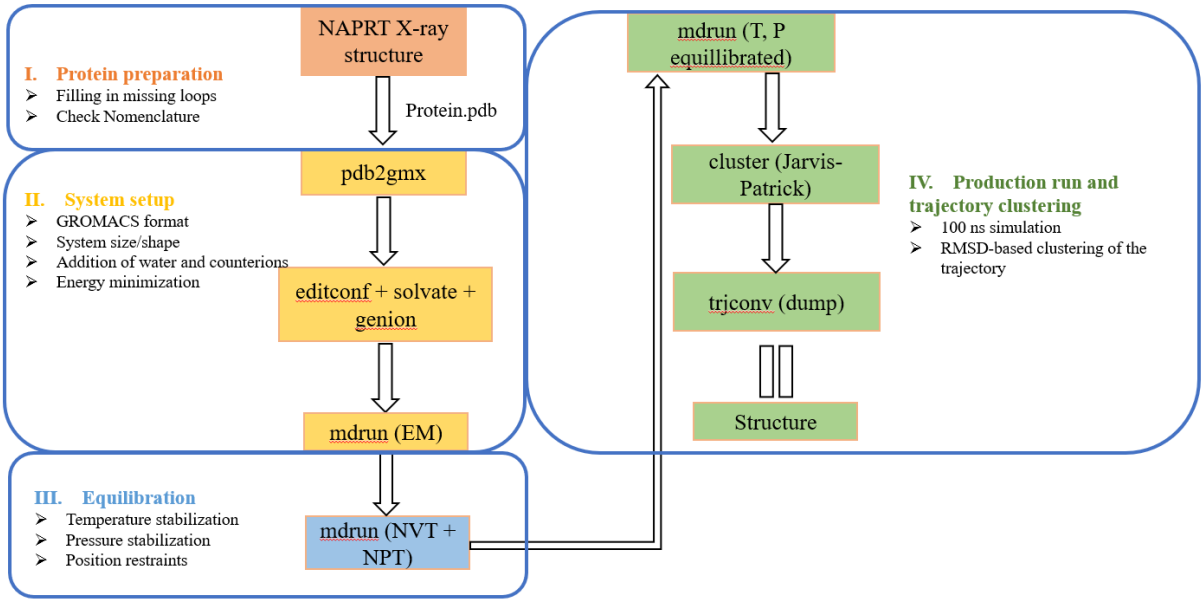

Figure 5. Steps undertaken to perform molecular dynamics simulation on NAPRT and postprocessing of data.

The chemical compounds that were subjected to docking screening were obtained from several sources. The list of libraries and providers is numbered below.

1. Approximately 1×10^5 molecules from the "Potentially purchasable compounds" Mcule database, selected based on simple physicochemical properties.
2. The Prestwick Chemical Library® [58].
3. Approximately 2000 in-stock compounds from EDASA Scientific [59].
4. A small selection of approximately 100 molecules that were synthesized by the University of Seville, some of which have already been described [60–62].
5. A small selection of compounds based on the *in vitro* results obtained from the first virtual screening docking hits (section 2.2.1).

Ligand preparation, docking and visual inspection of ligand-receptor binding poses were conducted as described in section 2.2.1. The most promising compounds (a total of 62 small molecules) were purchased or provided by collaborators and tested *in vitro*. Compounds were obtained in mg quantity and subsequently dissolved in DMSO to prepare a 50 mM stock solution. The purity of all compounds was > 95%, as declared by vendors or collaborators.

2.3 *In vitro* characterization of putative NAPRT inhibitors

2.3.1 Cell viability assay on the OVCAR-5 cell line

A total of 3×10^3 OVCAR-5 cells/well were plated in 96-well plates in the regular culture medium. 24 h later the cell medium was removed, and the cells were subsequently incubated either in the regular medium that was supplemented with 0.3 μM nicotinic acid (control wells) or in the treatment medium which contained 0.3 μM nicotinic acid and combinations of 100 nM FK866, 1 mM 2-HNA, and 100 μM of test compounds. Each condition was performed in triplicate and the cells remained under treatment for a total of 72 h at 37°C. Thereafter, the culture plates were fixed with 10% trichloroacetic acid at 4°C for 20 min, washed with cold water, and dried overnight. The plates were stained with 0.04% sulforhodamine B (SRB) in 1% acetic acid, washed four times with 1% acetic acid to remove the unbound dye, and dried overnight. Lastly, Trizma®-base 10 mM was added to the plates and cell viability was quantified by absorbance measurements on a Tecan Infinite® 200 PRO instrument.
To quantify the extent of the interaction between FK866 and the putative NAPRT inhibitors or 2-HNA, we applied the combination index (CI) equation that is depicted below:

$$\mathrm{CI} = \frac{mortality\ \%\ A + mortality\ \%\ B}{mortality\ \%\ (A + B)} \qquad (1)$$

where: '*A*' refers to the treatment of cells with FK866 100 nM; '*B*' refers to the treatment of cells with the test compound 100 μM or 2-HNA 1 mM; '*A* + *B*' refers to the coadministration of FK866 100 nM and the test compound at 100 μM or 2-HNA 1 mM. A synergistic interaction is evidenced by CI < 1, additive effect produces CI close to 1, whereas CI > 1 corresponds to antagonistic effect.

2.3.2 Ovcar-5 intracellular NAD^+ quantification

A total of 1×10^5 OVCAR-5 cells/well were plated in 24-well plates in the regular culture medium. 24 h later the cell medium was removed, and the cells were cultured either in the regular medium that was supplemented with 0.3 μM nicotinic acid (control wells) or in the treatment medium (regular medium with 0.3 μM nicotinic acid and combinations of 30 nM FK866, 1 mM 2-HNA and 100 μM of test compounds). Each condition was performed in duplicate, and the cells remained under treatment for a total of 20 h at 37°C. Thereafter, the

cell medium was removed, and the cells were harvested and lysed with 0.6 M perchloric acid (PCA). Samples in PCA were neutralized by diluting the extracts in 100 mM sodium phosphate buffer (pH 8) and the total intracellular NAD^+ content was determined with a sensitive enzyme cycling assay that exploits the use of alcohol dehydrogenase [63]. The obtained NAD^+ values were normalized to cell lysate protein content that was quantified by the Bradford method.

2.3.3 Inhibition assay on recombinant hNAPRT

The production of recombinant hNAPRT employed *E. coli* bacteria as an expression system. The human coding sequence for NAPRT was codon optimized for the expression in *E. coli* and cloned in a pET-23a vector containing a C-terminal His-tag by GenScript. A total of 5 ml of bacterial culture was grown overnight at 37°C in the Luria–Bertani medium that was supplemented with 100 µg/mL ampicillin. The day after the culture was diluted at 1:100 in fresh medium and incubated at 25°C. When a 0.3–0.4 OD_{600} was reached, protein expression was started at 20°C by adding 1 mM IPTG, followed by overnight incubation.

The induced cells were harvested by mild centrifugation (5000 rpm, 10 min) in a Beckman Coulter J6-HC centrifuge with JA-10 rotor and resuspended in 1:50 original volume with equilibrium buffer (100 mM K_2HPO_4, 300 mM KCl, and 5 mM imidazole, pH 7.4). After sonication (18 × 10 s), the crude extract was clarified by centrifugation (6000 rpm, 15 min) with JA-20 rotor, and purified by His-tag affinity chromatography as follows. The supernatant was batch-mixed (1 h) with a HisPur Cobalt resin (Thermo Fisher Scientific, Pittsburg, PA, USA), previously equilibrated in the above equilibrium buffer, and then packed into a chromatographic column. The flow-through and the subsequent 10 mM imidazole wash buffer were discarded. The recombinant protein was eluted by equilibration buffer containing 150 mM imidazole.

After centrifuge-assisted protein concentration in a Protein Concentrator 10K (Pierce-Thermo Fisher Scientific, Pittsburg, PA, USA), the hNAPRT amount was quantified by absorbance measurement at 280 nm. The solution containing the protein was dialyzed overnight against 50 mM Tris/HCl, pH 7.4, 10 mM KCl, and 1 mM DTT, to remove imidazole and change the buffer with the reaction buffer. To improve enzyme stability, after dialysis, 0.5 mM PRPP and 20% glycerol were added, and the protein was aliquoted and kept at −20 °C. All the steps were performed at 4°C.

hNAPRT was expressed in *E. coli* with an *N*-terminal His-tag and purified as described above. The enzymatic reactions were carried out at 37°C in standard reaction mixtures containing 50

mM Tris-HCl, pH 7.4, 10 mM KCl, 2 mM $MgCl_2$, 100 µM nicotinic acid, 200 µM PRPP, 0.1 mg/mL purified recombinant hNAPRT, and the test compound at five different concentrations ranging from 20 µM to 1000 µM.

Blank mixtures without compounds but with equal amounts of DMSO were set in parallel and their rates fixed as 100% activity. NAPRT was pre-incubated with the compounds for 5 min and reactions were started by the addition of the enzyme substrates and stopped after 45 min of incubation by heating to 85°C for 3 min. Following centrifugation of the reaction mix, the supernatant was analyzed by HPLC by injection into a reverse-phase column (XTerra MS C18 Column, 125Å, 5 µm, 4.6 × 150 mm, Waters). The eluted species were monitored at 260 nm and the peaks of nicotinic acid and nicotinic acid mononucleotide were quantified with reference to standard curves. The percentage of nicotinic acid conversion was calculated for each reaction and the IC_{50} values for the active compounds were determined with GraphPad Prism 8 software (GraphPad Software, S. Diego, CA, USA).

2.3.4 hNAPRT melting temperature determination

The melting temperature (Tm) of hNAPRT was determined through the differential scanning fluorimetry (DSF) technique. Triplicates of 100 µM of each test compound and DMSO were added to a 96-well clear bottom BioRad PCR plate. Subsequently, DSF protein buffer, containing 5 µM of recombinant hNAPRT protein and 5X SPYRO® Orange (S5692, Sigma-Aldrich) in 20 mM HEPES pH 7.5, 100 mM NaCl, 10 mM Mg-acetate, and 1 mM DTT was added. The plate was sealed and exposed to a temperature gradient from 20 to 95°C in a BioRad CFX96 Real-Time System. The fluorescence for each temperature increment was measured at 465–580 nm with an excitation wavelength of 465 nm. The DSF templates that were provided by Niesen et al. were used for data analysis followed by GraphPad Prism 8 for statistical analysis of the generated data [64].

3. RESULTS

For the development of NAPRT inhibitors, two main docking-based screenings of large and diverse compound libraries were performed. To maximize the chances to identify active molecules, one screening was run on the crystal structure conformation of the NAPRT active site whereas a suitable protein conformation generated through molecular dynamics simulation was used as the receptor in the second screening. For this reason, this section is divided into two parts, each describing the most relevant results from each virtual screening and subsequent *in vitro* characterization of the docking hits.

3.1 *In vitro* testing of the putative NAPRT inhibitors identified via NAPRT crystal structure active site conformation

3.1.1 Effect of compounds on recombinant hNAPRT enzymatic activity

The percentages of NAPRT inhibition for the most potent inhibitors identified through the first virtual screening are shown in Table 4. The putative hNAPRT inhibitors and the reference inhibitor of NAPRT (2-hydroxynicotinic acid) were assayed at a single concentration of 100 µM on the recombinant NAPRT.

Table 4. Percentage of enzymatic inhibition at a test compound concentration of 100 µM.

Code Name	NAPRT inhibition (%)
2-Hydroxynicotinic acid	**15.3**
IM4	30.3
IM11	28.5
MMB8-2	26.8
IM8	17.3
IM10	17.7
IM13	18.2
IM18	22.9

Strikingly, 7 compounds exhibited an improved NAPRT inhibition compared to 2-hydroxynicotinic acid, with the most potent inhibitors (IM4 and IM11) almost doubling the activity of the NAPRT substrate analogue.

In light of these promising results, the inhibitors cited in Table 4 were tested in combinations with FK866 on the NAPRT-proficient OVCAR-5 cell line, to discover whether the inhibition on the human NAPRT translated, for these specific compounds, into an anticancer activity.

3.1.2 Compounds-mediated sensitization of OVCAR-5 cells to FK866

This assay is set to identify NAPRT inhibitors that are able to replicate the ability of 2-HNA to sensitize OVCAR-5 cells to the NAMPT inhibitor, FK866.

None of the NAPRT inhibitors discovered in section 3.1.1 exerted at a compound concentration of 100 µM any degree of sensitization at the range of FK866 concentrations tested. The results obtained for the two most potent NAPRT inhibitors are shown in Figure 6.

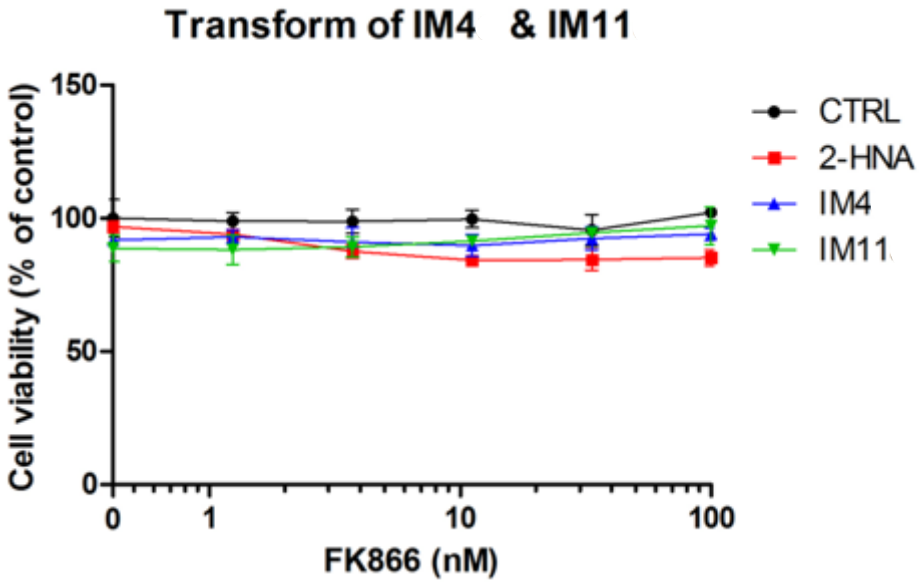

Figure 6. 2-HNA 100µM subtly sensitizes OVCAR-5 cells to FK866. OVCAR-5 cells were treated during 72h with combinations of 2-HNA or test compounds at 100 µM and FK866 ranging from 0 to 100 nM.

As observed, OVCAR-5 cell viability remained essentially invariable at any combination of IM4 + FK866 or IM11 + FK866. These were also the results obtained for the other five NAPRT inhibitors (MMB8-2, IM8, IM10, IM13 and IM18) (data not shown).

In contrast, the reference NAPRTi (2-hydroxynicotinic acid) exerts an increasing cell cytotoxicity at increasing concentrations of FK866, indicating that 2-HNA inhibits the NAPRT enzyme within the cells and sensitizes the otherwise FK866-resistant cell line.

Despite the outcome of the cell assay, the enzymatic activity assay on the recombinant NAPRT provides a very interesting result for the most potent inhibitors (IM4 and IM11).

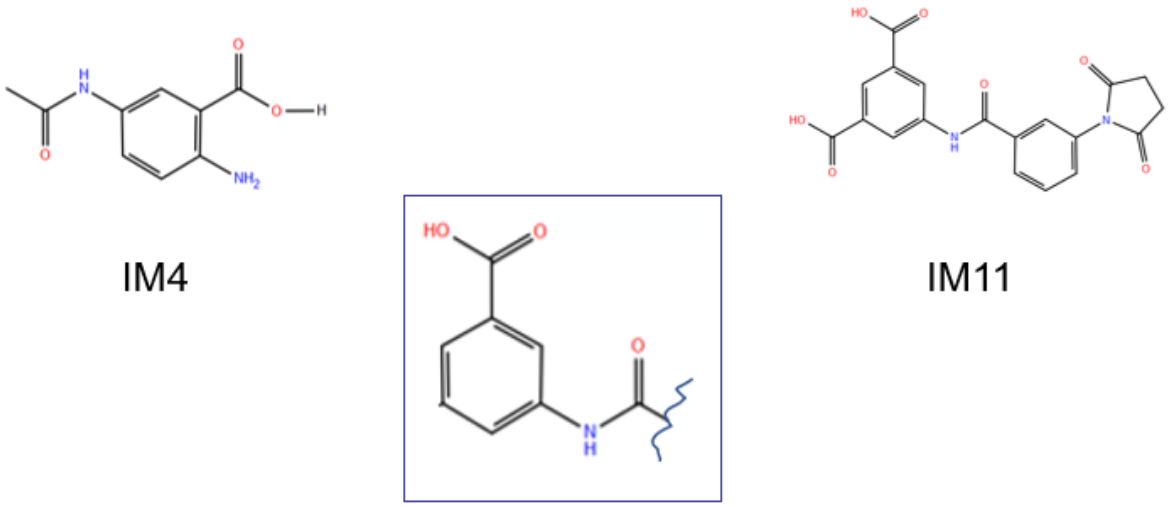

Figure 7. Structure of fragment present in compounds IM4 and IM11 which could be responsible for the activity observed.

Considering the structures of IM4 and IM11 and the fact that they inhibit NAPRT to a similar extent, it is reasonable to think that the moiety shared by them (Figure 7) could be responsible for the activity observed and deserves further testing. The fragment contained by both inhibitors consists of a benzoic acid with a secondary amide at position 3 (meta- position) and it was used as the input structure in substructure searches aimed at discovering NAPRT inhibitors with increased activity compared to IM4 and IM11 on OVCAR-5 cells.

3.2 Results for the putative NAPRT inhibitors identified via molecular dynamics simulations on NAPRT

In this section the results obtained from the vHTS on the simulated NAPRT are described. A comparison of the enzyme active site between the crystal structure and the conformation extracted from the molecular dynamics simulation is shown in Figure 8.

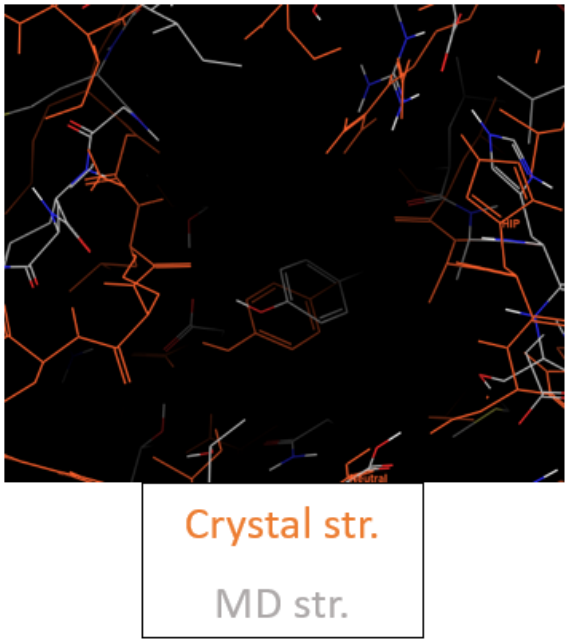

Figure 8. Superposition of the NAPRT active site conformations employed in the 1st and 2nd vHTS.

As it can be seen, the active site pocket in the frame extracted from the simulation is considerably more open compared to the active site in the NAPRT crystal structure.

The libraries docked in this second *in silico* screening contain a large number of diverse small molecules and a selection of ligands containing the moiety described in Figure 7. In total, 62 compounds advanced to *in vitro* testing.

The *in vitro* assays started with experiments on the OVCAR-5 cell line and then continued with on-target activity experiments on the recombinant NAPRT.

3.2.1 Sensitization of OVCAR-5 cells to FK866 as *in vitro* screening of putative NAPRT inhibitors

The first assay to test the putative NAPRT inhibitors was based on the principle that NAPRT-expressing OVCAR-5 cells are resistant to FK866 whereas the simultaneous chemical inhibition of NAPRT with 2-HNA renders the cells sensitive to the NAMPT inhibitor due to the cooperation between FK866 and 2-HNA in depleting the intracellular NAD pool [26]. It was observed that, in line with the work that was conducted by Piacente et al., OVCAR-5 cells withstood 72 h treatments with 100 nM FK866 or 1 mM 2-HNA, whereas co-treatment with both compounds at the specified concentrations resulted in a marked synergistic effect exerting pronounced cell death (Figure 9). Thus, 2-HNA was used throughout the study as a positive control in the cell viability assay and any test compound resembling its activity was considered a potential NAPRT inhibitor. It is worth mentioning that, to reflect the physiological

contribution of the Preiss–Handler pathway to NAD biosynthesis, all cell-based assays that are presented in this study were performed under a nicotinic acid concentration of 0.3 µM in the cell culture medium.

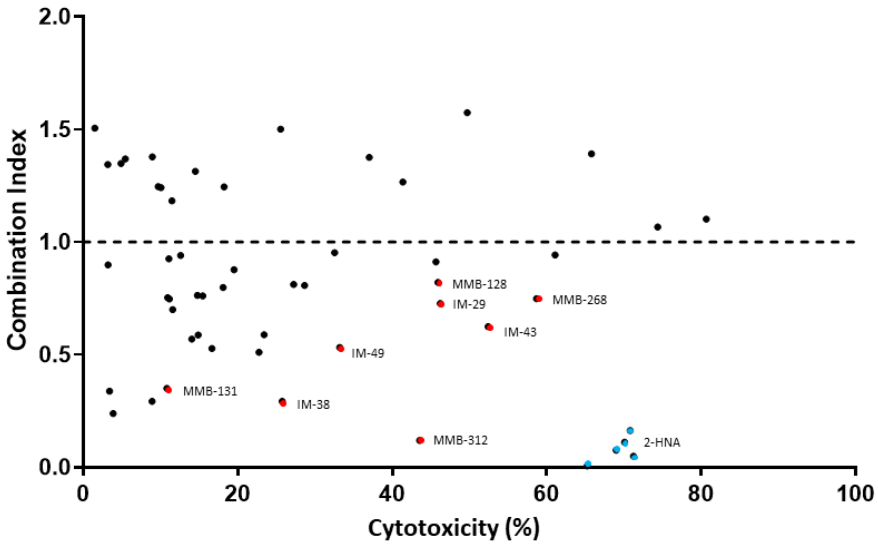

Figure 9. CI of compounds that were tested in combination with FK866 on OVCAR-5 cells. The cells were cultured in RPMI 1640 medium containing test compounds at a 100 µM concentration with and without 100 nM FK866 and the cell viability was determined following 72 h treatments. The data are shown as CI vs. cytotoxicity exerted on cells. Blue dots represent the reference NAPRT inhibitor, 2-HNA. Red dots belong to the best performing test compounds.

Combination index (CI) was used as a measure to determine the degree of interaction between FK866 and the test compounds, i.e., to identify potential new NAPRT inhibitors. A CI < 1 indicates a synergistic interaction between the test compound and FK866 in decreasing cell viability. A CI = 1 and a CI > 1 are indicative of an additive and of an antagonistic effect, respectively.

Figure 9 shows that the simultaneous administration of FK866 and 2-HNA produced the lowest CI out of all the combinations that were tested (CI = 0.08) and marked cytotoxicity. Among all the tested compounds, eight (represented by red dots in Figure 9) were considered to be especially interesting for their low CI or their high cytotoxicity when they were combined with FK866. Compounds IM 29, IM 43, MMB-128, and MMB-268 exhibited a CI ranging between 0.62 and 0.82 and high cytotoxicity in combination with FK866 and these results might suggest other interactions within the cells while some degree of synergism (CI < 1) with FK866 was evident, suggesting the inhibition of the Preiss–Handler NAD biosynthetic pathway.

Compounds IM 38, IM 49, MMB-131, and MMB-312 produced less pronounced cytotoxicity when they were combined with FK866. However, this subset of compounds showed especially low combination indexes ($0.12 \leq CI \leq 0.53$) and, therefore, a larger synergism with FK866.

These eight compounds were all considered promising candidates for NAPRT inhibition and were selected for further *in vitro* assays.

3.2.2 Effect of test compounds on intracellular OVCAR-5 NAD^+ levels

The assay that was performed on OVCAR-5 cell viability led to a set of potential NAPRT inhibitors, namely IM 29, IM 38, IM 43, IM 49, MMB-128, MMB-131, MMB-268, and MMB-312. In order to confirm that the cited compounds sensitized OVCAR-5 cells to the NAMPT inhibitor FK866 by interfering with NAD biosynthesis, the intracellular NAD^+ levels in OVCAR-5 cells were quantified after 20 h treatments with these compounds with or without FK866.

As Figure 10 shows, treatment with 30 nM FK866 alone decreased the NAD^+ levels by 24%. The effect of FK866 was strongly enhanced when the drug was combined with 1 mM 2-HNA, yielding an 86 % drop in the intracellular NAD^+ concentration, thus evidencing marked synergism between the two compounds in depleting NAD^+. This observation is in line with the fact that the combination of FK866 and 2-HNA achieved the lowest CI and the highest cytotoxicity in the cell viability studies.

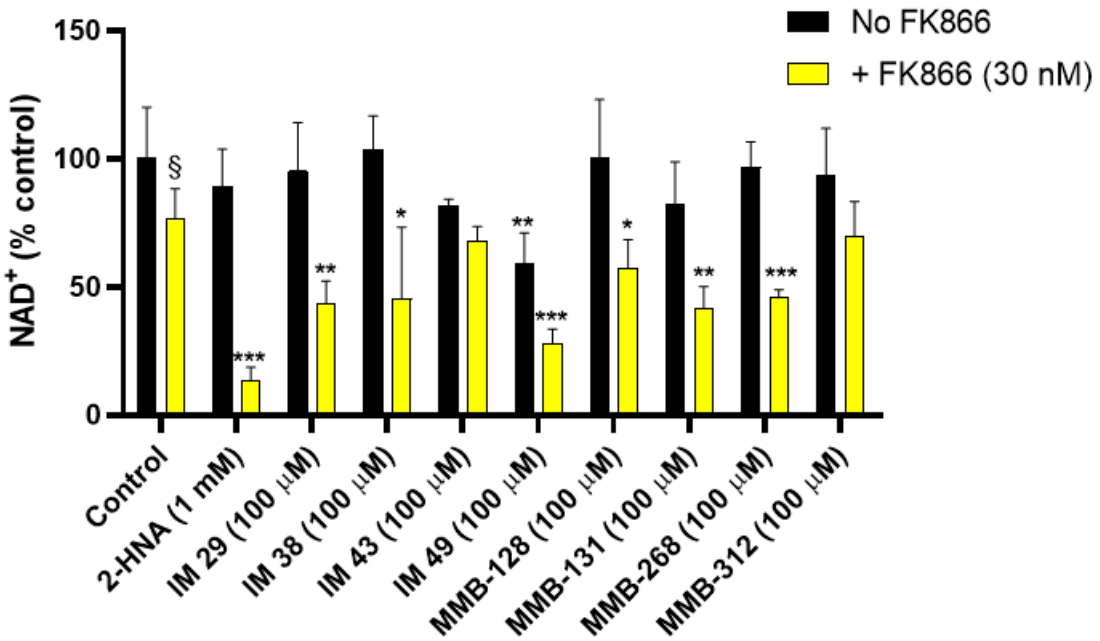

*Figure 10. A subset of test compounds cooperates synergistically with FK866 in decreasing intracellular NAD^+ levels in OVCAR-5 cells. The compounds were administered to cells alone or in combination with FK866 for 20 h. Quantification of NAD^+ was performed via an enzyme cycling assay and normalized to cell lysate protein content. The results are the mean ± SD of two technical replicates with two biological replicates each. *, $p < 0.05$; **, $p < 0.01$; ***, $p < 0.001$ vs. the respective control, i.e., FK866-untreated control for the test compounds that were administered alone to cells, and FK866-treated control for the combinations of test compound and FK866; §, $p < 0.05$ versus FK866-untreated, control cells.*

In keeping with the cell viability experiments, the test compounds IM 29, IM 38, MMB-128, MMB-131, and MMB-268 were found to mimic the effect of 2-HNA on intracellular NAD^+ levels and thus represent a set of potential NAPRT inhibitors. Indeed, co-treatments with the cited compounds at a 100 μM concentration and 30 nM FK866 produced a marked drop in the NAD^+ levels (42.9–56.4%). A similar decrease in NAD^+ was obtained in response to the NAMPT inhibitor combined with compound IM 49. Nevertheless, compound IM 49 by itself strongly reduced the OVCAR-5 intracellular NAD^+ levels. Therefore, a lower degree of synergism was observed between this test compound and FK866. Possibly, IM 49 can interfere with other enzyme(s) that are involved in NAD synthesis in addition to hNAPRT.

Besides the test compounds that effectively cooperate with FK866 in decreasing NAD^+ levels, the co-administration of compounds IM 43 and MMB-312 with FK866 only yielded additive effects in terms of NAD^+ reduction in OVCAR-5 cells. As depicted in Figure 10, cotreatments with the cited compounds and FK866 did not cause a major reduction of the NAD^+ levels. These results appear not to be in line with the cell viability assay, where IM 43 exerted high cytotoxicity in combination with FK866 in OVCAR-5 cells, while MMB-312 achieved the lowest CI value (CI = 0.12) out of all the tested compounds. These results suggest that other mechanisms may come into play to justify the synergy between IM 43 or MMB-312 and FK866, which need to be addressed in further studies.

3.2.3 On-target activity of test compounds: inhibition of the recombinant hNAPRT

The six test compounds that were found to exert a synergistic effect with FK866 on OVCAR-5 intracellular NAD^+ levels were tested in a biochemical assay with recombinant hNAPRT as inhibitors of the enzyme catalytic activity. These inhibition studies resulted in the identification of five new hNAPRT inhibitors with IC_{50} values in the micromolar range. Compound IM 29 exhibited the highest activity against the formation of nicotinic acid mononucleotide with an IC_{50} of 160 μM (Figure 11). Comparable results were obtained for compounds IM 38, IM 49, MMB-128, and MMB-131, with estimated IC_{50} in the 200–300 μM range. This enzymatic assay confirmed that the observed cooperation between FK866 and the tested compounds in decreasing OVCAR-5 cell viability and intracellular NAD^+ levels was due to the ability of the compounds to inhibit NAPRT. Noteworthy, compound MMB-268 showed negligible inhibition of NAPRT (data not shown).

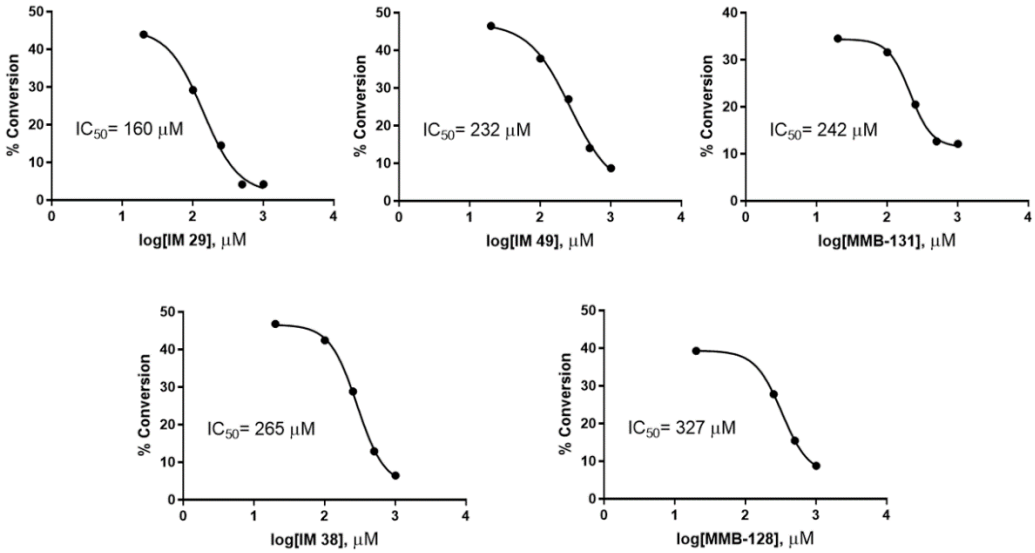

Figure 11. Compounds IM 29, IM 49, MMB-131, IM 38, and MMB-128 inhibit recombinant hNAPRT in the μM range. The test compounds were added at different concentrations to reaction mixtures containing hNAPRT and substrates and the half maximal inhibitory concentration (IC_{50}) was obtained for each compound by measuring the amounts of NA and NAMN that were present after the reactions.

3.2.4 On-target activity of test compounds: effect on hNAPRT melting temperature

With the purpose to provide support to the results that were obtained in the enzymatic activity assay, the ability of the new NAPRT inhibitors to stabilize the protein through binding was evaluated via the measurement of the NAPRT melting temperature in the presence or absence of the inhibitors at a 100 μM concentration. The resulting Tm shifts are depicted in Figure 12. Interestingly, a significant positive shift by approximately 0.5°C in the Tm of hNAPRT was induced by compounds MMB-128 and MMB-131, suggesting a certain affinity of the inhibitors towards the protein that results in thermal stabilization. On the contrary, the melting temperature of hNAPRT remained unchanged when the enzyme was exposed to compounds IM 29, IM 38, or IM 49. A plausible explanation for this outcome is that larger compounds are more likely to establish a higher number of interactions and thus result in greater stabilization of a given protein. Indeed, significant Tm shifts were reached with the two largest inhibitors (MMB-128 and MMB-131).

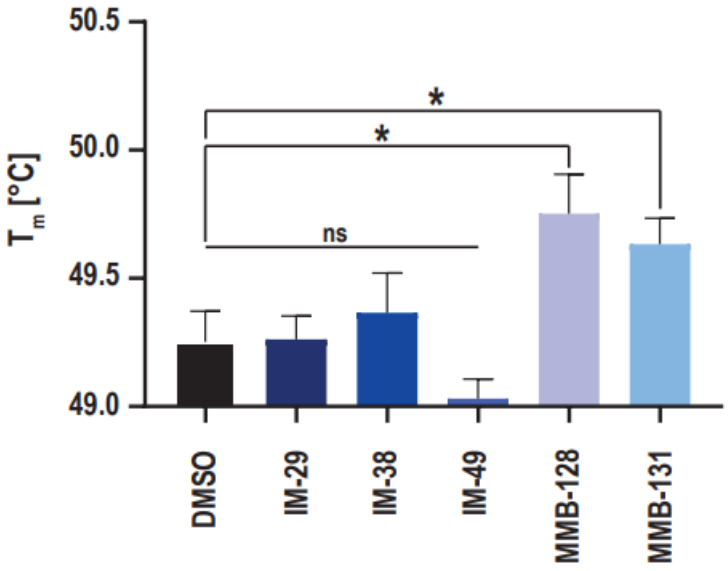

*Figure 12. NAPRT inhibitors MMB-128 and MMB-131 directly engage recombinant hNAPRT. Differential scanning fluorimetry (DSF) was used to determine the thermal stabilization of hNAPRT protein upon inhibitor binding. Recombinant hNAPRT protein was exposed to 100 μM hNAPRT inhibitors over a defined temperature gradient and the melting temperature Tm was calculated for each compound. The data are shown as means ± standard error of the means (SEM) of two technical replicates with three biological replicates each. * $p < 0.05$; unpaired t-test.*

3.2.5 Retrospective analysis of the hNAPRT inhibitors binding in the active site

Following the *in vitro* characterization of the new NAPRT inhibitors, a molecular docking on the NAPRT structure was performed to shed light on the binding mode features that are likely related to the enzyme inhibition. Docking of compound IM 29 shows that the small and rigid molecule binds deep into the active site pocket of hNAPRT and it is stabilized by several interactions with protein residues (Figure 13A, B). Remarkably, IM 29 establishes two pi-cation contacts with ARG318A, a residue that is reported to exert a key role in catalysis that is potentially hampered by IM 29 binding [24,25]. The ionization at a physiological pH of the amino group of IM 29 appears relevant for engagement and inhibition of hNAPRT. Indeed, the carboxylate side chain of GLU167A in proximity to the ammonium moiety of IM 29 indicates suitable ligand-receptor electrostatic complementarity and results in a salt bridge and short-distance hydrogen bond between the cited amino acid and the hNAPRT inhibitor.

As for compound IM 29, docking into the NAPRT active site provides a favorable binding mode for IM 38. Of note, compound IM 38 was selected from the substructure searches inspired in compounds IM4 and IM11, identified in the first vHTS. The ligand fits in the active site maintaining the inherent planarity of its amide conjugated system, resulting in negligible ligand strain. Electrostatic potential mapping of the protein (Figure 13C) shows that the most electronegative atoms of the inhibitor are surrounded by positively charged active site residues.

As for many drug candidates in medicinal chemistry, the affinity of NAPRT towards IM 38 is largely explainable by the occurrence of numerous hydrogen bonds upon ligand binding. The carboxylate moiety of the ligand is key for its bioactivity, participating in two H-bonds with the backbone of NAPRT residues HIS213A and SER214A (Figure 13D). Furthermore, through its amide and ether groups, IM 38 establishes several hydrogen bonds with the amino acids ARG318A and LEU170A. The latter residue also interacts with the chlorine atom of IM 38, albeit the poor directionality of the halogen bond suggests this interaction to be of limited relevance.

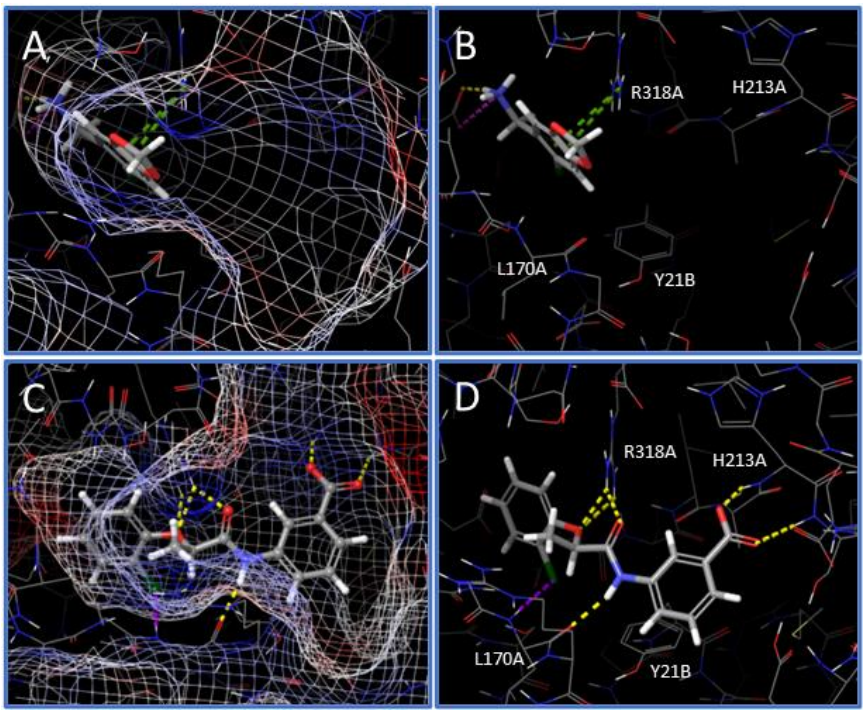

*Figure 13. Binding mode that is predicted by molecular docking of compounds IM 29 (**A**,**B**) and IM 38 (**C**,**D**) in the hNAPRT active site. The analysis of the docking binding poses was performed on the academic version of Schrodinger Maestro v.2017-4. Protein is represented in thin sticks whereas ligands are depicted in thick tubes. Hydrogen bonds appear as yellow dotted lines. Salt bridges are represented by pink dotted lines. Pi-cation interactions are depicted as green dotted lines and halogen bonds are shown as purple dotted lines.*

4. DISCUSSION

Since NAD depletion emerged as a promising anticancer strategy, most of the research has focused on disabling the nicotinamide salvage pathway, which overall represents the main route to NAD biosynthesis in mammals. Indeed, several families of potent NAMPT inhibitors have emerged over the last decades with encouraging preclinical antitumor efficacy. Unfortunately, the expectations on some of these NAMPT inhibitors were not met later in clinical trials, which showed limited clinical activity for these compounds. Piacente et al. hypothesized that alternative NAD production routes could represent a mechanism of tumor resistance to NAMPT inhibitors and demonstrated that the Preiss–Handler pathway gene NAPRT is frequently amplified and overexpressed in a subset of human tumors such as ovarian, breast, pancreatic, and prostate cancer. In the cited study, targeting NAPRT through silencing or chemical inhibition with 2-HNA effectively sensitized NAPRT-expressing cancer cells to FK866 both *in vitro* and *in vivo*. In addition, the authors highlighted the need to discover new NAPRT inhibitors with increased potency with respect to 2-hydroxynicotinic acid and other active compounds that date back to the last century.

This study employs a variety of structure-based drug design approaches coupled to cell and enzymatic assays to evaluate the bioactivity of the putative NAPRT inhibitors.

In the absence of known potent NAPRT inhibitors, the search for active compounds was not restricted to a particular scaffold or chemical space. Therefore, the compound libraries subjected to the two docking-based virtual screenings comprised large numbers of diverse, drug-like compounds. The ultimate goal was to pave the way for the development of a new generation of NAPRT inhibitors that improve the potency of the reference NAPRT inhibitor in anticancer research, 2-hydroxynicotinic acid.

The docking hits from the first vHTS resulted in the identification of a few inhibitors with similar or better potency compared to 2-HNA on recombinant NAPRT enzymatic activity.

Of note, these new inhibitors were not able to sensitize the NAPRT-proficient OVCAR-5 cells to FK866 in terms of cell viability. This means that the new compounds are not endowed with the antitumor activity that characterizes 2-HNA. Having demonstrated on-target activity by inhibiting NAPRT, it is hypothesized that:

1) the test compounds lack cell membrane permeability, i.e., they are unable to inhibit the intracellular target (NAPRT).

2) the test compounds are not stable inside the cell and are degraded.

Nevertheless, the two most potent compounds (IM4 and IM11) from this pool of newly identified NAPRT inhibitors happen to share an interesting fragment in their structure that is probably responsible for the inhibitory activity on NAPRT. Thus, this fragment was subjected to substructure search to discover molecules that at least maintain the inhibitory activity of IM4 and IM11 on NAPRT while enhancing the cytotoxicity on the OVCAR-5 cell line.

Molecular dynamics simulations were run on NAPRT to generate the docking grid around the enzyme active site for the second docking-based virtual screening. This provided a suitable NAPRT active site conformation that constitutes an alternative to the NAPRT crystal structure. The *in silico* hits from this second screening were experimentally tested through a workflow of *in vitro* assays that prioritized the early identification of compounds that recapitulated the effects of 2-HNA on OVCAR-5 cells. Accordingly, the first assays quantified the effects of compounds on cell viability and intracellular NAD^+ levels. Then, the on-target activity on the recombinant NAPRT was demonstrated by enzymatic assays and binding to NAPRT was assessed through measurements of the NAPRT melting temperature (Tm).

A total of eight compounds (Table 5) demonstrated synergism along with FK866 in decreasing cell viability, suggesting an impairment of the Preiss–Handler pathway. Most of these hits also showed the ability to cooperate with FK866 synergistically to decrease intracellular NAD^+ levels in OVCAR-5 cells. Specifically, such an effect on intracellular NAD^+ was observed in response to six compounds (IM 29, IM 38, IM 49, MMB-128, MMB-131, and MMB-268) when these were combined with FK866. Conversely, two compounds (IM 43 and MMB-312) showed promising results in the cell viability assay but failed to cooperate with FK866 to lower the NAD^+ levels, suggesting that their antitumor effect may reflect an off-target activity.

Out of the six compounds that moved on to the next assay, five of them (IM 29, IM 38, IM 49, MMB-128, and MMB-131) showed inhibitory properties against hNAPRT with IC_{50} in the micromolar range. A remarkable result is that IM 38 is a product of the substructure searches effectuated on the previously identified IM4 and IM11 (see Table 6 for structures). As desired, IM 38 maintained the inhibition on NAPRT and most importantly, was able to exert anticancer effects on OVCAR-5 cells. The suitability of the sequence of assays conducted is supported by the fact that only one compound (MMB-268) out of the pool of candidates that exerted NAPRTi-like behavior in cell assays failed to inhibit hNAPRT enzymatic activity. Finally, the capability of the hNAPRT inhibitors herein identified to confer thermal stability to hNAPRT was investigated by DSF. Direct engagement of compounds MMB-128 and MMB-131 to NAPRT was confirmed by positive shifts in the protein melting temperature when exposed to the inhibitors. An explanation for the lack of significant results for the other NAPRTi (IM 29,

IM 38, and IM 49) in the Tm assay might reside in the composition of the incubation mixture. In fact, the assay was performed in the absence of the natural NAPRT substrates. This means that the inhibitors that possess a mechanism of action in which substrate binding is necessary for posterior inhibitor binding, will not show activity in the conditions of the assay.

As shown in Table 5, in summary, the reported findings broaden the chemical space of known hNAPRT inhibitors and pave the way for the identification of new NAD-lowering anticancer drugs targeting NAPRT-expressing malignancies. The new hNAPRT inhibitors described are able to inhibit the recombinant NAPRT enzyme with comparable or improved potency *versus* 2-HNA. The compounds also show synergy with FK866 in decreasing OVCAR-5 cell viability and NAD^+ content. Moreover, the new NAPRT inhibitors are characterized by a low molecular weight and, thus, are susceptible to undergo optimization studies to increase their activity through structure modifications.

Table 5. Advancement of the best NAPRTi identified in the sequence of in vitro assays. Green = desired activity. Red = insufficient activity/not tested.

Compound	**Cell viability (OVCAR-5)**		**NAD^+ depletion+FK866 (%)**	**NAPRT IC_{50} (µM)**	**ΔT_m (˚C)**
	CI	Cytotoxicity+FK866 (%)			
IM 29	0.73	46	56	160	0.01
IM 38	0.29	26	55	265	0.12
IM 43	0.62	52	32	Not tested	Not tested
IM 49	0.53	33	72	232	-0.22
MMB-128	0.82	46	43	327	0.5
MMB-131	0.35	11	58	242	0.38
MMB-268	0.75	59	54	No inhibition	Not tested
MMB-312	0.12	44	31	Not tested	Not tested

Table 6. Chemical structures of the best NAPRTi discovered and inhibitors IM4 and IM11.

Best NAPRT inhibitors identified	Structure
IM 29	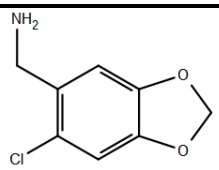
MMB-128	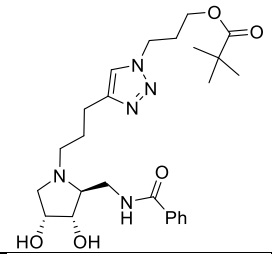
IM 38	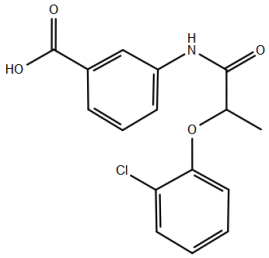
MMB-131	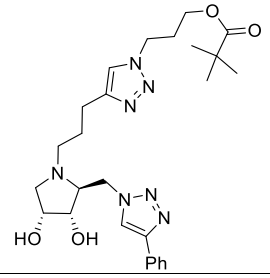
IM 49	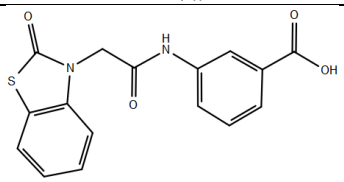
IM4	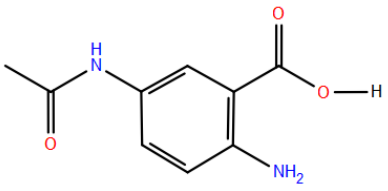
IM11	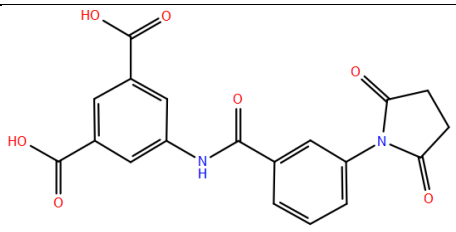

5. REFERENCES

1. Yang, Y.; Sauve, A.A. NAD+ Metabolism: Bioenergetics, Signaling and Manipulation for Therapy. *Biochim Biophys Acta Proteins Proteom* 2016, *1864*, 1787–1800.
2. Cantó, C.; Menzies, K.J.; Auwerx, J. NAD+ Metabolism and the Control of Energy Homeostasis: A Balancing Act between Mitochondria and the Nucleus. *Cell Metab* 2015, *22*, 31–53.
3. Navas, L.E.; Carnero, A. NAD+ Metabolism, Stemness, the Immune Response, and Cancer. *Signal Transduct Target Ther* 2021, *6*.
4. Agledal, L.; Niere, M.; Ziegler, M. The Phosphate Makes a Difference: Cellular Functions of NADP. *Redox Report* 2010, *15*, 2–10.
5. Lin, H. Nicotinamide Adenine Dinucleotide: Beyond a Redox Coenzyme. *Org Biomol Chem* **2007**, *5*, 2541–2554, doi:10.1039/b706887e.
6. Covarrubias, A.J.; Perrone, R.; Grozio, A.; Verdin, E. NAD+ Metabolism and Its Roles in Cellular Processes during Ageing. *Nat Rev Mol Cell Biol* 2021, *22*, 119–141.
7. Houtkooper, R.H.; Cantó, C.; Wanders, R.J.; Auwerx, J. The Secret Life of NAD+: An Old Metabolite Controlling New Metabolic Signaling Pathways. *Endocr Rev* 2010, *31*, 194–223.
8. Berger, N.A.; Besson, V.C.; Boulares, A.H.; Bürkle, A.; Chiarugi, A.; Clark, R.S.; Curtin, N.J.; Cuzzocrea, S.; Dawson, T.M.; Dawson, V.L.; et al. Opportunities for the Repurposing of PARP Inhibitors for the Therapy of Non-Oncological Diseases. *Br J Pharmacol* 2018, *175*, 192–222.
9. Houtkooper, R.H.; Pirinen, E.; Auwerx, J. Sirtuins as Regulators of Metabolism and Healthspan. *Nat Rev Mol Cell Biol* 2012, *13*, 225–238.
10. Quarona, V.; Zaccarello, G.; Chillemi, A.; Brunetti, E.; Singh, V.K.; Ferrero, E.; Funaro, A.; Horenstein, A.L.; Malavasi, F. CD38 and CD157: A Long Journey from Activation Markers to Multifunctional Molecules. *Cytometry B Clin Cytom* 2013, *84*, 207–217.
11. Essuman, K.; Summers, D.W.; Sasaki, Y.; Mao, X.; DiAntonio, A.; Milbrandt, J. The SARM1 Toll/Interleukin-1 Receptor Domain Possesses Intrinsic NAD+ Cleavage Activity That Promotes Pathological Axonal Degeneration. *Neuron* **2017**, *93*, 1334-1343.e5, doi:10.1016/j.neuron.2017.02.022.
12. Chiarugi, A.; Dölle, C.; Felici, R.; Ziegler, M. The NAD Metabolome - A Key Determinant of Cancer Cell Biology. *Nat Rev Cancer* 2012, *12*, 741–752.
13. Zapata-Pérez, R.; Wanders, R.J.A.; Karnebeek, C.D.M.; Houtkooper, R.H. NAD + Homeostasis in Human Health and Disease . *EMBO Mol Med* **2021**, *13*, doi:10.15252/emmm.202113943.
14. Pramono, A.A.; Rather, G.M.; Herman, H.; Lestari, K.; Bertino, J.R. NAD-and NADPH-Contributing Enzymes as Therapeutic Targets in Cancer: An Overview. *Biomolecules* 2020, *10*.
15. Yaku, K.; Okabe, K.; Hikosaka, K.; Nakagawa, T. NAD Metabolism in Cancer Therapeutics. *Front Oncol* 2018, *8*.
16. Nagro, C. del; Xiao, Y.; Rangell, L.; Reichelt, M.; O'Brien, T. Depletion of the Central Metabolite NAD Leads to Oncosismediated Cell Death. *Journal of Biological Chemistry* **2014**, *289*, 35182–35192, doi:10.1074/jbc.M114.580159.
17. Ghanem, M.S.; Monacelli, F.; Nencioni, A. Advances in Nad-Lowering Agents for Cancer Treatment. *Nutrients* **2021**, *13*, doi:10.3390/nu13051665.
18. Nikiforov, A.; Dölle, C.; Niere, M.; Ziegler, M. Pathways and Subcellular Compartmentation of NAD Biosynthesis in Human Cells: From Entry of Extracellular

Precursors to Mitochondrial NAD Generation. *Journal of Biological Chemistry* **2011**, *286*, 21767–21778, doi:10.1074/jbc.M110.213298.
19. Lau, C.; Niere, M.; Ziegler, M. The NMN/NaMN Adenylyltransferase (NMNAT) Protein Family. *Frontiers in Bioscience* **2009**, *14*, 410–431, doi:10.2741/3252.
20. Rongvaux, A.; Andris, F.; van Gool, F.; Leo, O. Reconstructing Eukaryotic NAD Metabolism. *BioEssays* 2003, *25*, 683–690.
21. Duarte-Pereira, S.; Pereira-Castro, I.; Silva, S.S.; Correia, M.G.; Neto, C.; da Costa, L.T.; Amorim, A.; Silva, R.M. Extensive Regulation of Nicotinate Phosphoribosyltransferase (NAPRT) Expression in Human Tissues and Tumors. *Oncotarget* **2016**, *7*, 1973–1983, doi:10.18632/oncotarget.6538.
22. Gossmann, T.I.; Ziegler, M.; Puntervoll, P.; de Figueiredo, L.F.; Schuster, S.; Heiland, I. NAD+ Biosynthesis and Salvage - A Phylogenetic Perspective. In Proceedings of the FEBS Journal; September 2012; Vol. 279, pp. 3355–3363.
23. Hara, N.; Yamada, K.; Shibata, T.; Osago, H.; Tsuchiya, M. Nicotinamide Phosphoribosyltransferase/Visfatin Does Not Catalyze Nicotinamide Mononucleotide Formation in Blood Plasma. *PLoS One* **2011**, *6*, doi:10.1371/journal.pone.0022781.
24. Marletta, A.S.; Massarotti, A.; Orsomando, G.; Magni, G.; Rizzi, M.; Garavaglia, S. Crystal Structure of Human Nicotinic Acid Phosphoribosyltransferase. *FEBS Open Bio* **2015**, *5*, 419–428, doi:10.1016/j.fob.2015.05.002.
25. Galassi, L.; di Stefano, M.; Brunetti, L.; Orsomando, G.; Amici, A.; Ruggieri, S.; Magni, G. Characterization of Human Nicotinate Phosphoribosyltransferase: Kinetic Studies, Structure Prediction and Functional Analysis by Site-Directed Mutagenesis. *Biochimie* **2012**, *94*, 300–309, doi:10.1016/j.biochi.2011.06.033.
26. Piacente, F.; Caffa, I.; Ravera, S.; Sociali, G.; Passalacqua, M.; Vellone, V.G.; Becherini, P.; Reverberi, D.; Monacelli, F.; Ballestrero, A.; et al. Nicotinic Acid Phosphoribosyltransferase Regulates Cancer Cell Metabolism, Susceptibility to NAMPT Inhibitors, and DNA Repair. *Cancer Res* **2017**, *77*, 3857–3869, doi:10.1158/0008-5472.CAN-16-3079.
27. Duarte-Pereira, S.; Fajarda, O.; Matos, S.; Oliveira, J.L.; Silva, R.M. Naprt Expression Regulation Mechanisms: Novel Functions Predicted by a Bioinformatics Approach. *Genes (Basel)* **2021**, *12*, doi:10.3390/genes12122022.
28. Chowdhry, S.; Zanca, C.; Rajkumar, U.; Koga, T.; Diao, Y.; Raviram, R.; Liu, F.; Turner, K.; Yang, H.; Brunk, E.; et al. NAD Metabolic Dependency in Cancer Is Shaped by Gene Amplification and Enhancer Remodelling. *Nature* **2019**, *569*, 570–575, doi:10.1038/s41586-019-1150-2.
29. Olesen, U.H.; Hastrup, N.; Sehested, M. Expression Patterns of Nicotinamide Phosphoribosyltransferase and Nicotinic Acid Phosphoribosyltransferase in Human Malignant Lymphomas. *APMIS* **2011**, *119*, 296–303, doi:10.1111/j.1600-0463.2011.02733.x.
30. Hara, N.; Yamada, K.; Shibata, T.; Osago, H.; Hashimoto, T.; Tsuchiya, M. Elevation of Cellular NAD Levels by Nicotinic Acid and Involvement of Nicotinic Acid Phosphoribosyltransferase in Human Cells. *Journal of Biological Chemistry* **2007**, *282*, 24574–24582, doi:10.1074/jbc.M610357200.
31. Audrito, V.; Messana, V.G.; Deaglio, S. NAMPT and NAPRT: Two Metabolic Enzymes With Key Roles in Inflammation. *Front Oncol* 2020, *10*.
32. Managò, A.; Audrito, V.; Mazzola, F.; Sorci, L.; Gaudino, F.; Gizzi, K.; Vitale, N.; Incarnato, D.; Minazzato, G.; Ianniello, A.; et al. Extracellular Nicotinate Phosphoribosyltransferase Binds Toll like Receptor 4 and Mediates Inflammation. *Nat Commun* **2019**, *10*, doi:10.1038/s41467-019-12055-2.

33. Hasmann, M.; Schemainda, I. FK866, a Highly Specific Noncompetitive Inhibitor of Nicotinamide Phosphoribosyltransferase, Represents a Novel Mechanism for Induction of Tumor Cell Apoptosis. *Cancer Res* **2003**, *63*, 7436–7442.
34. Olesen, U.H.; Christensen, M.K.; Björkling, F.; Jäättelä, M.; Jensen, P.B.; Sehested, M.; Nielsen, S.J. Anticancer Agent CHS-828 Inhibits Cellular Synthesis of NAD. *Biochem Biophys Res Commun* **2008**, *367*, 799–804, doi:10.1016/j.bbrc.2008.01.019.
35. Sampath, D.; Zabka, T.S.; Misner, D.L.; O'Brien, T.; Dragovich, P.S. Inhibition of Nicotinamide Phosphoribosyltransferase (NAMPT) as a Therapeutic Strategy in Cancer. *Pharmacol Ther* 2015, *151*, 16–31.
36. Korotchkina, L.; Kazyulkin, D.; Komarov, P.G.; Polinsky, A.; Andrianova, E.L.; Joshi, S.; Gupta, M.; Vujcic, S.; Kononov, E.; Toshkov, I.; et al. OT-82, a Novel Anticancer Drug Candidate That Targets the Strong Dependence of Hematological Malignancies on NAD Biosynthesis. *Leukemia* **2020**, *34*, 1828–1839, doi:10.1038/s41375-019-0692-5.
37. Aboud, O.A.; Chen, C.H.; Senapedis, W.; Baloglu, E.; Argueta, C.; Weiss, R.H. Dual and Specific Inhibition of NAMPT and PAK4 by KPT-9274 Decreases Kidney Cancer Growth. *Mol Cancer Ther* **2016**, *15*, 2119–2129, doi:10.1158/1535-7163.MCT-16-0197.
38. Zhou, S.J.; Bi, T.Q.; Qin, C.X.; Yang, X.Q.; Pang, K. Expression of NAMPT Is Associated with Breast Invasive Ductal Carcinoma Development and Prognosis. *Oncol Lett* **2018**, *15*, 6648–6654, doi:10.3892/ol.2018.8164.
39. Olesen, U.H.; Thougaard, A. v.; Jensen, P.B.; Sehested, M. A Preclinical Study on the Rescue of Normal Tissue by Nicotinic Acid in High-Dose Treatment with APO866, a Specific Nicotinamide Phosphoribosyltransferase Inhibitor. *Mol Cancer Ther* **2010**, *9*, 1609–1617, doi:10.1158/1535-7163.MCT-09-1130.
40. Tarrant, J.M.; Dhawan, P.; Singh, J.; Zabka, T.S.; Clarke, E.; Dossantos, G.; Dragovich, P.S.; Sampath, D.; Lin, T.; McCray, B.; et al. Preclinical Models of Nicotinamide Phosphoribosyltransferase Inhibitor-Mediated Hematotoxicity and Mitigation by Co-Treatment with Nicotinic Acid. *Toxicol Mech Methods* **2015**, *25*, 201–211, doi:10.3109/15376516.2015.1014080.
41. O'Brien, T.; Oeh, J.; Xiao, Y.; Liang, X.; Vanderbilt, A.; Qin, A.; Yang, L.; Lee, L.B.; Ly, J.; Cosino, E.; et al. Supplementation of Nicotinic Acid with NAMPT Inhibitors Results in Loss of in Vivo Efficacy in NAPRT1-Deficient Tumor Models. *Neoplasia (United States)* **2013**, *15*, 1314–1329, doi:10.1593/neo.131718.
42. Goldinger, S.M.; Bischof, S.G.; Fink-Puches, R.; Klemke, C.D.; Dréno, B.; Bagot, M.; Dummer, R. Efficacy and Safety of Apo866 in Patients with Refractory or Relapsed Cutaneous T-Cell Lymphoma: A Phase 2 Clinical Trial. *JAMA Dermatol* 2016, *152*, 837–839.
43. von Heideman, A.; Berglund, Å.; Larsson, R.; Nygren, P.; Larsson, R. Safety and Efficacy of NAD Depleting Cancer Drugs: Results of a Phase i Clinical Trial of CHS 828 and Overview of Published Data. *Cancer Chemother Pharmacol* **2010**, *65*, 1165–1172, doi:10.1007/s00280-009-1125-3.
44. Piacente, F.; Caffa, I.; Nencioni, A. Nicotinic Acid: A Case for a Vitamin That Moonlights for Cancer? *Cell Cycle* 2017, *16*, 1635–1636.
45. Tateishi, K.; Wakimoto, H.; Iafrate, A.J.; Tanaka, S.; Loebel, F.; Lelic, N.; Wiederschain, D.; Bedel, O.; Deng, G.; Zhang, B.; et al. Extreme Vulnerability of IDH1 Mutant Cancers to NAD+ Depletion. *Cancer Cell* **2015**, *28*, 773–784, doi:10.1016/j.ccell.2015.11.006.
46. Lee, J.; Kim, H.; Lee, J.E.; Shin, S.J.; Oh, S.; Kwon, G.; Kim, H.; Choi, Y.Y.; White, M.A.; Paik, S.; et al. Selective Cytotoxicity of the NAMPT Inhibitor FK866 Toward

Gastric Cancer Cells With Markers of the Epithelial-Mesenchymal Transition, Due to Loss of NAPRT. *Gastroenterology* **2018**, *155*, 799-814.e13, doi:10.1053/j.gastro.2018.05.024.
47. Fons, N.R.; Sundaram, R.K.; Breuer, G.A.; Peng, S.; McLean, R.L.; Kalathil, A.N.; Schmidt, M.S.; Carvalho, D.M.; Mackay, A.; Jones, C.; et al. PPM1D Mutations Silence NAPRT Gene Expression and Confer NAMPT Inhibitor Sensitivity in Glioma. *Nat Commun* **2019**, *10*, doi:10.1038/s41467-019-11732-6.
48. Franceschini, N.; Oosting, J.; Tamsma, M.; Niessen, B.; Briaire-De Bruijn, I.; van den Akker, B.; Kruisselbrink, A.B.; Palubeckait˙, I.; Bovée, J.V.M.G.; Cleton-Jansen, A.-M.; et al. Targeting the NAD Salvage Synthesis Pathway as a Novel Therapeutic Strategy for Osteosarcomas with Low NAPRT Expression. *International Journal of Molecular Sciences Article J. Mol. Sci* **2021**, doi:10.3390/ijms.
49. Watson, M.; Roulston, A.; Bélec, L.; Billot, X.; Marcellus, R.; Bédard, D.; Bernier, C.; Branchaud, S.; Chan, H.; Dairi, K.; et al. The Small Molecule GMX1778 Is a Potent Inhibitor of NAD + Biosynthesis: Strategy for Enhanced Therapy in Nicotinic Acid Phosphoribosyltransferase 1-Deficient Tumors . *Mol Cell Biol* **2009**, *29*, 5872–5888, doi:10.1128/mcb.00112-09.
50. Kudo, K.; Nomura, M.; Sakamoto, Y.; Ito, S.; Morita, M.; Kawai, M.; Yamashita, Y.; Ito, K.; Yamada, H.; Shima, H.; et al. Divergent Metabolic Responses Dictate Vulnerability to NAMPT Inhibition in Ovarian Cancer. *FEBS Lett* **2020**, *594*, 1379–1388, doi:10.1002/1873-3468.13736.
51. Gaut, Z.N.; Solomon, H.M. Inhibition of 7- 14 C-Nicotinic Acid Metabolism in the Human Blood Platelet by Anti-Inflammatory Drugs. *Res Commun Chem Pathol Pharmacol* **1970**, *1*, 547–552.
52. Gaut, Z.N.; Solomon, H.M. Inhibition of Nicotinate Phosphoribosyltransferase in Human Platelet Lysate by Nicotinic Acid Analogs. *Biochem Pharmacol* **1971**, *20*, 2903–2906, doi:10.1016/0006-2952(71)90202-4.
53. Gaut, Z.N.; Solomon, H.M. Inhibition of Nicotinate Phosphoribosyl Transferase by Nonsteroidal Anti-Inflammatory Drugs: A Possible Mechanism of Action. *J Pharm Sci* **1971**, *60*, 1887–1888, doi:10.1002/jps.2600601230.
54. Www.Rcsb.Org.
55. Ropp, P.J.; Spiegel, J.O.; Walker, J.L.; Green, H.; Morales, G.A.; Milliken, K.A.; Ringe, J.J.; Durrant, J.D. GypSUm-DL: An Open-Source Program for Preparing Small-Molecule Libraries for Structure-Based Virtual Screening. *J Cheminform* **2019**, *11*, doi:10.1186/s13321-019-0358-3.
56. Www.Mcule.Com.
57. Fischer, A.; Smieško, M.; Sellner, M.; Lill, M.A. Decision Making in Structure-Based Drug Discovery: Visual Inspection of Docking Results. *J Med Chem* 2021, *64*, 2489–2500.
58. Www.Prestwickchemical.Com.
59. Www.Edasascientific.Com.
60. Martínez-Bailén, M.; Galbis, E.; Carmona, A.T.; de-Paz, M.V.; Robina, I. Preparation of Water-Soluble Glycopolymers Derived from Five-Membered Iminosugars. *Eur Polym J* **2019**, *119*, 213–221, doi:10.1016/j.eurpolymj.2019.07.027.
61. Martínez-Bailén, M.; Carmona, A.T.; Moreno-Clavijo, E.; Robina, I.; Ide, D.; Kato, A.; Moreno-Vargas, A.J. Tuning of β-Glucosidase and α-Galactosidase Inhibition by Generation and in Situ Screening of a Library of Pyrrolidine-Triazole Hybrid Molecules. *Eur J Med Chem* **2017**, *138*, 532–542, doi:10.1016/j.ejmech.2017.06.055.
62. Martínez-Bailén, M.; Carmona, A.T.; Patterson-Orazem, A.C.; Lieberman, R.L.; Ide, D.; Kubo, M.; Kato, A.; Robina, I.; Moreno-Vargas, A.J. Exploring Substituent

Diversity on Pyrrolidine-Aryltriazole Iminosugars: Structural Basis of β-Glucocerebrosidase Inhibition. *Bioorg Chem* **2019**, *86*, 652–664, doi:10.1016/j.bioorg.2019.02.025.
63. Bruzzone, S.; de Flora, A.; Usai, C.; Graeff, R.; Lee, H.C. Cyclic ADP-Ribose Is a Second Messenger in the Lipopolysaccharide-Stimulated Proliferation of Human Peripheral Blood Mononuclear Cells. *Biochemical Journal* **2003**, *375*, 395–403, doi:10.1042/bj20030556.
64. Niesen, F.H.; Berglund, H.; Vedadi, M. The Use of Differential Scanning Fluorimetry to Detect Ligand Interactions That Promote Protein Stability. *Nat Protoc* **2007**, *2*, 2212–2221, doi:10.1038/nprot.2007.321.

ACKNOWLEDGEMENTS

First, I would like to thank Dr. Alberto Del Rio, managing director at Innovamol Consulting Srl, who gave me the chance to work on this PhD thesis and provided his supervision and immense support throughout these years. I would also like to express my gratitude to Prof. Dr. Alessio Nencioni, who provided constant guidance and discussion of my thesis results and made the INTEGRATA project possible. This project was funded by the European Union's Horizon 2020 research and innovation program under grant agreement No 81328 (INTEGRATA). I also appreciate the support and feedback from the INTEGRATA consortium members and PhD fellows. I also sincerely express my gratitude to the following people who have had a great contribution to this thesis:

- A very special thanks to my colleagues at the DI.M.I and DI.M.ES departments of the University of Genova. Dr. Francesco Piacente, Prof. Dr. Santina Bruzzone and Dr. Irene Caffa for their invaluable help in designing, performing, and interpreting the *in vitro* assays.

Also thanks to Andrea Benzi, Moustafa Ghanem, Maria Elena Laugieri and Amr Khalifa for their support in my lab experiments.

- Simone Fratta, Irene Conforti and their supervisors at the University of Sevilla and the University of Montpellier for providing compounds to test on NAPRT.
- Dr. Daniele Tedesco and Dr. Marco Daniele Parenti for their training on computer-aided drug design theory and practical applications.
- Melanie Walter and her supervisors at the University of Sheffield for testing the effect of NAPRT inhibitors on the melting temperature of the enzyme.
- Andrea Altieri and Alexander V. Kurkin for facilitating virtual compound libraries and samples to test in the lab as putative NAPRT inhibitors.

Roberta Chiodini and Greta Varchi of Innovamol Consulting Srl for their warm welcome and all the moments shared.

I would also like to thank and wish the best to all my INTEGRATA PhD fellows. Lastly, I thank my family and friends, who have provided great support.